Mean stream coordinates structure of the Subantarctic Front: Temperature, salinity, and absolute velocity

Christopher S. Meinen,[1,2] Douglas S. Luther,[1] D. Randolph Watts,[3] Alan D. Chave,[4] and Karen L. Tracey[3]

Received 17 July 2002; revised 1 April 2003; accepted 28 May 2003; published 15 August 2003.

[1] The mean synoptic structure of the northern, strongest branch of the Antarctic Circumpolar Current southwest of Tasmania, at the Subantarctic Front (SAF), is estimated by a stream coordinates analysis of data from overlapping arrays of Inverted Echo Sounders (IESs) and Horizontal Electric Field Recorders deployed during the 1995–1997 Sub-Antarctic Flux and Dynamics Experiment. The stream coordinates are derived from a daily objective mapping of the temperature field obtained from combining the IES travel time measurements with an empirical look-up table constructed from the extensive hydrography acquired during WOCE. Full-water-column stream-coordinates sections of temperature, Salinity, and absolute velocity are presented and compared with prior observations. The along-stream current has a single peak with surface velocities reaching about 50 cm s^{-1}. The vertical structure of the along-stream velocity is roughly consistent with a combined external and first internal normal mode description that is adapted to the buoyancy frequency as it varies across the front, although there are some significant differences. The cross-stream structure of along-stream velocity is very nearly symmetric about the jet axis, but the lateral shear magnitude is slightly larger on the cold side of the SAF. Separating the baroclinic and barotropic currents reveals that the SAF currents are diffluent, primarily baroclinically, in the cross-stream direction. Baroclinic cross-stream diffluence of approximately 0.23 Sv per km (Sv = 10^6 m^3 s^{-1}), or about 16 Sv per degree of longitude at 51°S. The 2-year mean total SAF transport is 75 Sv (for a 220 km width); the barotropic contribution is small (8 Sv) but not negligible. *INDEX TERMS:* 4207 Oceanography: General: Arctic and Antarctic oceanography; 4512 Oceanography: Physical: Currents; 4528 Oceanography: Physical: Fronts and jets; 4532 Oceanography: Physical: General circulation; *KEYWORDS:* Subantarctic Front, Antarctic Circumpolar Current, Southern Ocean, stream coordinates, SAF, ACC

Citation: Meinen, C. S., D. S. Luther, D. R. Watts, A. D. Chave, and K. L. Tracey, Mean stream coordinates structure of the Subantarctic Front: Temperature, salinity, and absolute velocity, *J. Geophys. Res.*, *108*(C8), 3263, doi:10.1029/2002JC001545, 2003.

1. Introduction

[2] Historically, in situ observations of the Antarctic Circumpolar Current (ACC) have been limited by the inhospitable weather and sea-state conditions in the Southern Ocean during much of the year. The most heavily observed region of the ACC has been at the Drake Passage, because the natural constriction there permits a reasonable expectation of capturing the total transport of the ACC with the fewest moored instruments or with the smallest amount of ship time [e.g., *Bryden*, 1979; *Nowlin and Klinck*, 1986]. A small number of densely instrumented field programs have focused on the dynamics and energetics of other portions of the ACC, for example, south of New Zealand [*Bryden and Heath*, 1985], south of Africa [*Whitworth and Nowlin*, 1987], and south of Australia [*Phillips and Rintoul*, 2000, 2002], while satellite measurements have been used to study the ACC pathways [e.g., *Gille*, 1994; *Park and Gamberoni*, 1995; *Moore et al.*, 1997] and surface dynamics [e.g., *Chelton et al.*, 1990; *Mestas-Nunez et al.*, 1992; *Morrow et al.*, 1994; *Moore et al.*, 1999]. This list is not meant to be exhaustive; a recent review by *Rintoul et al.* [2001] presents many aspects of the current state of knowledge of the ACC system and gives a more complete listing of the observational studies which have taken place up through the mid-1990s.

[3] The flow which makes up the ACC is divided primarily between transport along two fronts; the Polar

[1]Department of Oceanography, University of Hawaii at Manoa, Honolulu, Hawaii, USA.
[2]Cooperative Institute for Marine and Atmospheric Studies, University of Miami, Miami, Florida, USA.
[3]Graduate School of Oceanography, University of Rhode Island, Narragansett, Rhode Island, USA.
[4]Deep Submergence Laboratory, Applied Ocean Physics and Engineering, Woods Hole Oceanographic Institution, Woods Hole, Massachusetts, USA.

0148-0227/03/2002JC001545$09.00

Front and the Subantarctic Front [*Orsi et al.*, 1995; *Rintoul et al.*, 2001]. South of Australia the majority of the ACC flow is along the Subantarctic Front (SAF [*Rintoul et al.*, 2001]), the focus of this paper. Except for within the Drake Passage, direct measurements of absolute water velocities along the SAF are rare. Numerous hydrographic studies have been completed, however, providing basic information about the baroclinic structure and variability of the SAF [e.g., *Orsi et al.*, 1995]. The geostrophic relative velocities from six hydrographic sections across the ACC in the Pacific sector of the Southern Ocean were absolutely referenced using shipboard acoustic Doppler current profiler data, thus providing a few absolute velocity snapshots of the SAF [*Donohue et al.*, 2001]. In the early 1990s, a 2-year study utilizing four current meter moorings (the AUSSAF array) was completed south of Australia [*Phillips and Rintoul*, 2000, 2002]. These moored velocity measurements provided the first look at the mean absolute velocity structure of the SAF south of Australia.

[4] A larger study, the Sub-Antarctic Flux and Dynamics Experiment (SAFDE), was accomplished during 1995–1997 south of Australia. The SAFDE included a large array of Inverted Echo Sounders (IESs) and Horizontal Electric Field Recorders (HEFRs) within which was also embedded a smaller array of traditional current meter moorings [*Luther et al.*, 1997]. Figure 1 presents the location and orientation of the array. Also shown in Figure 1 are the vertical-mean, time-averaged, geostrophic velocities relative to the bottom, derived from the IES data (discussed below). The mean SAF and Polar Front (PF) positions determined by *Gille* [1994] from GEOSAT sea-surface height gradients for 1986–1989 are illustrated as well. Notice that the IES-derived velocities have two separate peak directions, with the northern sites flowing toward the northeast while the southern sites indicate flow toward the east-southeast. These two peaks correspond to the latitudes where *Gille* [1994] defined the SAF and PF. *Sokolov and Rintoul* [2002] refer to a velocity maximum near 53°S as a southern branch of the SAF; the data presented herein are insufficient to prove whether the southern branch observed in Figure 1 represents an artifact of eddy processes, a separate branch of the SAF, or if it is the PF. Regardless of what one calls the southern flow, the purpose of this paper is to focus on the northern of these two flows, which we shall refer to as the SAF. Keep in mind, however, that the existence of the second front will influence the results on the southern side of the SAF when the two fronts are sufficiently close together.

[5] One purpose of SAFDE was to observe the combined baroclinic and barotropic synoptic mean ACC flow along the SAF. Because any individual snapshot section across the SAF, or any other strongly meandering frontal current, can be "contaminated" by meanders, eddies and other smaller-scale processes, the method generally used to obtain the synoptic mean structure of the current is the stream coordinates approach. "Stream coordinates" describes a coordinate system wherein location is defined not as a distance relative to a fixed point on the Earth but relative to some unique characteristic of the current, such as the velocity core. Orientation in stream coordinates is based on the direction of flow at the current core rather than on the compass directions of east and north. Stream coordinates techniques have been applied to a number of strong current

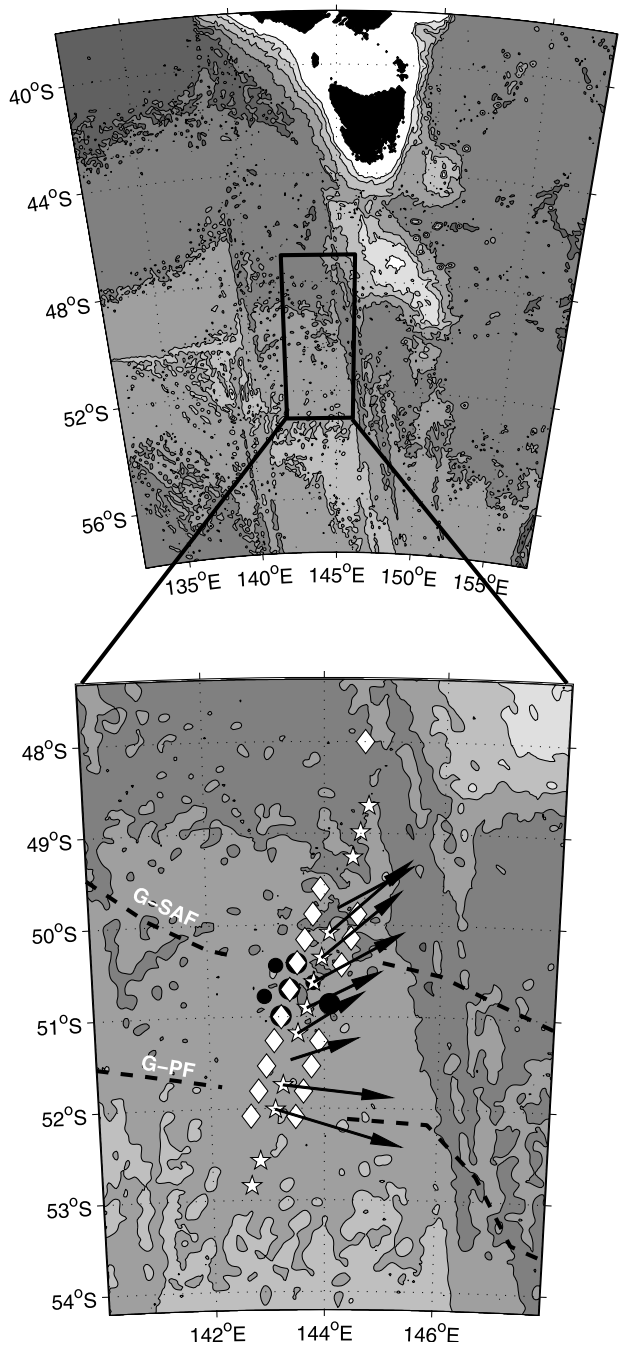

Figure 1. Location of the SAFDE array. White diamonds, white stars, large black circles, and small black circles indicate IES, HEFR, tall current meter mooring, and short current meter mooring locations, respectively. Bottom topography from *Smith and Sandwell* [1997] is denoted by shading at a contour interval of 1000 m; most of the SAFDE array region is 3000- to 4000-m deep. Black areas indicate land. Arrows represent the vertical mean, time-averaged, geostrophic velocities relative to the bottom, as derived from the IES data. The IES data are used here since HEFRs are not available for referencing at two locations within the array. It is shown in the text that the mean bottom velocities are small. The mean SAF and PF positions determined by *Gille* [1994] from GEOSAT sea-surface height gradients for 1986–1989 are shown as thick dashed lines (G-SAF and G-PF, respectively).

systems around the world, such as the Gulf Stream [*Halkin and Rossby*, 1985; *Hall*, 1986; *Hogg*, 1992; *Johns et al.*, 1995; *Bower and Hogg*, 1996], the North Atlantic Current [*Meinen*, 2001], the Kuroshio extension [*Hall*, 1989], and the Subantarctic Front [*Phillips and Rintoul*, 2002]. The details of the application of stream coordinates (such as the nature of a priori assumptions about the current's structure) in these studies differ, and for dynamical interpretations these differences can be important. *Meinen and Luther* [2003], hereinafter referred to as ML03, present a comparison of different stream coordinates techniques using the SAFDE data set. The present paper follows the method recommended in ML03 and provides a mean synoptic view of the temperature, salinity, and absolute velocity structure of the SAF. The method simply averages the observations based on the position and orientation of an indicator believed to be near the center of the front, without making any other a priori assumptions about the structure and variability of the front. The paper will also discuss some of the dynamical implications of the estimated stream coordinates mean sections.

2. Data

[6] The SAFDE experiment involved a large array of IESs, HEFRs, and current meters deployed over the period March 1995 through April 1997 (Figure 1). Good data were returned from 17 IESs, 12 HEFRs, and 17 current meters on seven moorings. Conductivity-temperature-depth (CTD) profiles were obtained in the SAFDE region on six WOCE SR3 cruises [*Rintoul and Sokolov*, 2001] and two SAFDE cruises; two WOCE cruises occurred during the SAFDE period. The present study focuses on the measurements made by the 16 IESs and 7 HEFRs which were located within the main array. Additionally, the three temperature-pressure sensor pairs (from 300 m to 1000 m) on the eastern mooring were used to create a pseudo-IES travel time record to fill a gap in the eastern IES line, following the methods presented by *Meinen and Watts* [2000].

[7] An IES is about 0.6-m tall and is moored about 1 m off the ocean bottom. It transmits a 10-kHz sound pulse and measures the time (τ) for the pulse to travel to the ocean surface and back [*Watts and Rossby*, 1977; *Chaplin and Watts*, 1984]. Using historical hydrography from the region of study, characteristic relationships between τ and other oceanic variables (e.g., temperature, salinity, specific volume anomaly) can be developed and combined with the IES measured τ to estimate full water column profiles of these variables [*Meinen and Watts*, 2000; *Watts et al.*, 2001]. The characteristic relationships are referred to as the "Gravest Empirical Modes," or GEMs, and there are separate GEM representations for temperature, salinity, and specific volume anomaly. The implication of the success of the GEM representation is that subinertial baroclinic variations of temperature and salinity at all depths are rather tightly linked in the SAF, although this does not imply that the vertical structure follows a particular dynamical mode structure (see *Watts et al.* [2001] for more discussion). Vertically integrating the specific volume anomaly profiles provides profiles of geopotential height anomaly that when differenced horizontally between neighboring IESs yield profiles of the relative velocity using the geostrophic (dynamic) method. Two-dimensional arrays of IESs can provide both components (north and east) of velocity.

[8] The HEFR measures the horizontal electric field induced by the ions in seawater moving through the magnetic field of Earth [e.g., *Sanford*, 1971; *Chave and Luther*, 1990; *Luther et al.*, 1991]. Because seawater is conductive, the electric fields short out in the vertical, and as a result the field measured by the HEFR represents the vertical mean of the horizontal field induced by the moving water. With proper calibration, this electric field is interpreted as the vertically averaged horizontal water velocity. Optimal interpolation (OI [*Bretherton et al.*, 1976]) is used to extract relative velocity profiles at each HEFR site from the IES array data, and then the HEFR measurements are used to reference the relative velocity profiles (see *Meinen et al.* [2002] for details). In combination, time series of full-water-column absolute velocity profiles are obtained at each HEFR site within the main array. Because of the OI mapping of the IES measurements, as well as the natural spatial integration inherent in the HEFR measurement [see *Chave and Luther*, 1990], the resulting velocities represent horizontal averages over a distance of roughly 30 km. Figure 2 shows time series of absolute velocity at five pressure levels at the site of HEFR 10 (seventh star from the top in Figure 1). While, on average, the barotropic flow, here defined as the near-bottom velocity [*Fofonoff*, 1962], is small, at times the deep velocities exceeded 10 cm s^{-1} for more than a week. This illustrates the importance of the absolute velocity referencing provided by the HEFRs.

[9] The calibration of the HEFRs in the SAFDE experiment is presented by A. D. Chave et al. (Correction of motional electric field measurements for galvanic distortion, submitted to *Journal of Atmospheric and Oceanic Technology*, 2003). The development of the characteristic hydrography relationships (GEM fields) and the combination with IES measurements followed the methods presented by *Meinen and Watts* [2000]. All measurement time series were low-pass filtered with a 72-hour second-order Butterworth filter, passed both backward and forward to avoid phase shifting, to eliminate tides and other high-frequency signals. The complete details of how the SAFDE IES and HEFR measurements were combined to provide daily (noon UT) time series of absolute velocity profiles have been presented by *Meinen et al.* [2002].

3. Motivation and Methods

[10] The motivation for describing strong oceanic currents in a stream coordinates reference frame, as opposed to Eulerian, has been widely discussed [*Halkin and Rossby*, 1985; *Hall*, 1986; *Rossby*, 1987; *Hall*, 1989; *Hogg*, 1992; *Johns et al.*, 1995; *Bower and Hogg*, 1996; *Kontoyiannis*, 1997; *Meinen*, 2001]. The analysis impediments arising from an Eulerian coordinate system result from two facts: The cores of strong oceanic currents shift laterally and they change direction relative to fixed geographic coordinates. Both of these facts lead to significant difficulty in interpreting, and making dynamical inferences from, measurements of fronts and their highly sheared currents using instruments moored at fixed locations. To illustrate the problem, Figure 3 shows nine daily maps of the depth of the 6°C isotherm (Z_6) within the array, demonstrating some of the different paths

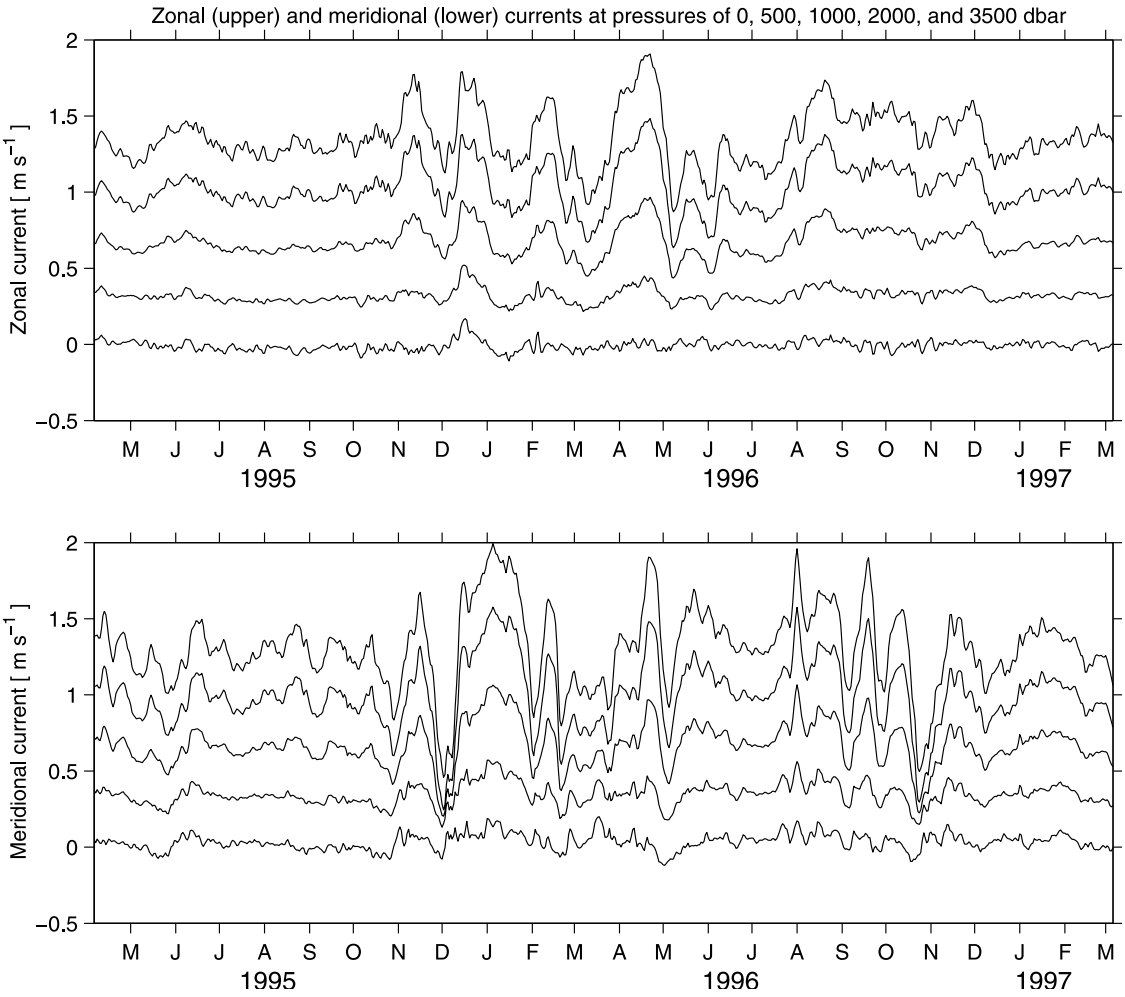

Figure 2. Absolute currents at five pressure levels at the site of HEFR 10 (seventh star from the top of Figure 1). (top) Zonal current component. (bottom) Meridional component. Pressure levels are 0, 500, 1000, 2000, and 3500 dbar; each time series except the 3500-dbar level has been offset upward by 0.3 m s^{-1} to avoid cluttering the figure.

which the SAF took across the array during the experiment. These maps of isotherm depth were determined by combining 10 km × 10 km resolution daily OI maps of IES measured travel times with the GEM temperature field to determine daily vertical temperature profiles, from which Z_6 is then extracted [*Meinen and Watts*, 2000; *Watts et al.*, 2001; *Meinen et al.*, 2002]. The core of the SAF front, which is defined as the location where the 6°C isotherm crosses 500 dbar, is denoted by the thick line. This definition of the SAF core is based on hydrographic measurements from the area and is discussed in detail in ML03. During the 2-year SAFDE (March 1995 to April 1997), the SAF crossed the array in a broad range of directions: towards the east (e.g., October 4, 1996); toward the north (e.g., January 6, 1996); and toward the south (e.g., December 4, 1995). At times when there were large meanders or rings in the front, there were even significant westward components to the flow (e.g., August 3, 1996). Moreover, at times these same meanders and rings resulted in the SAF crossing the array in more than one location.

[11] The conversion from Eulerian to stream coordinates has three main steps: determining a stream coordinates origin, determining the distance from each measurement site to the stream coordinates origin, and determining the direction of downstream flow (in order to rotate the eastward and northward velocities into along-stream and cross-stream components). ML03 used the SAFDE data sets to test several different methods for determining the cross-stream distance and downstream angle and have demonstrated that the resultant current structure depends upon the method chosen. One popular method assumes that lateral shifts (meanders) of a current enable observations from a single fixed mooring to profile across the current; this method is commonly referred to as the ''frozen field''

Figure 3. (opposite) Examples of OI maps of 6°C isotherm depths (Z_6) as determined by the IESs. See text for explanation of the calculation. Contour values are pressure in dbar. Thick line shows the 500-dbar contour. Dotted line indicates the border of the OI mapping region.

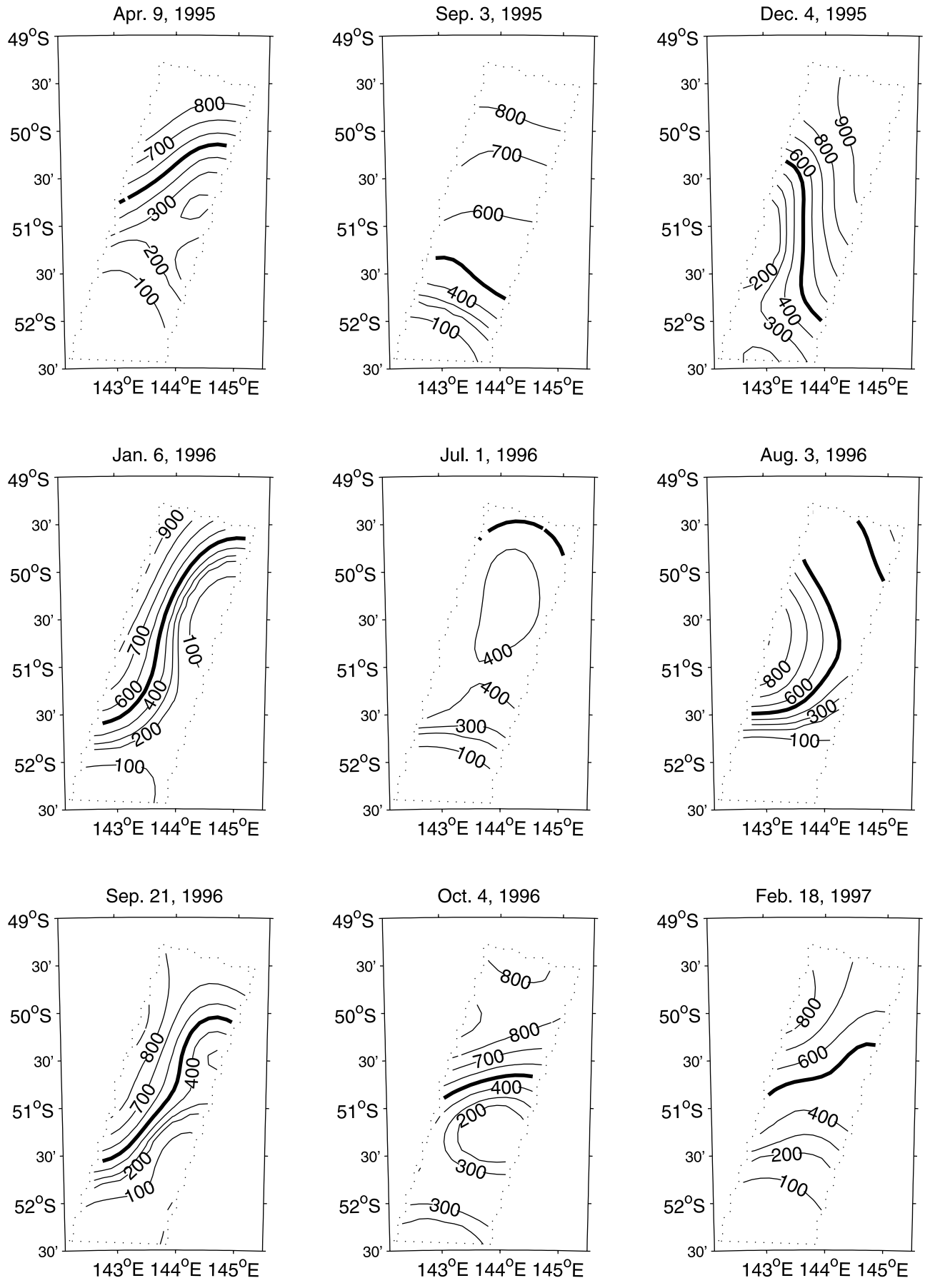
Apr. 9, 1995
Sep. 3, 1995
Dec. 4, 1995
Jan. 6, 1996
Jul. 1, 1996
Aug. 3, 1996
Sep. 21, 1996
Oct. 4, 1996
Feb. 18, 1997
49°S
30'
50°S
30'
51°S
30'
52°S
30'
143°E 144°E 145°E

method. Frozen field is defined here as a time-invariant relationship between density on a pressure surface, for example, and cross-stream location. The frozen field can be applied either directly to the daily velocity observations or to the time-mean velocities averaged in density bins (the order of time-averaging application is not important as averaging is a linear process). In the single mooring technique, downstream direction is defined as the direction which maximizes the vertical shear of the horizontal velocity; this shall be referred to as the ''vertical shear'' method.

[12] The methods suitable for lateral profiling by single moorings were not used in this study. Instead, the conversion from Eulerian to stream coordinates took advantage of the daily mapping of the current structure along the whole transect (resulting in an estimated mean structure with about 5 times as many degrees of freedom), and proceeded as follows. For each day of the time series, Z_6 was contoured through the array using the IES data. Then the closest approach of the Z_6 = 500 dbar contour (X_{Z6}) to each HEFR site was determined. Whenever possible, a line perpendicular to the Z_6 = 500 dbar contour and connecting the HEFR site to X_{Z6} was found. If successful, X_{Z6} was defined as the location of the SAF core for that HEFR site for that day. The distance between the two points was defined as the cross-stream distance (positive if the 6°C isotherm at the HEFR site was deeper than 500 dbar, negative if it was shallower), while the tangent to the Z_6 = 500 dbar contour line at X_{Z6} provided the direction of downstream flow for the rotation of the velocities into along-stream and cross-stream components. This procedure was repeated for each of the seven HEFR within the main array for each day. For situations where X_{Z6} was less than 3 km away, the distance was set to 0 km and the tangent at X_{Z6} provided the definition of downstream. Of the 4907 absolute velocity profiles (7 HEFR sites times 701 days), 3100 could be used in determining the stream coordinates mean. For the remaining site days the closest approach of the SAF was determined to be either outside the IES array or was very ambiguous, and as such the cross-stream location could not be reliably found. The usable velocity estimates, as well as the temperature and salinity estimates at those sites determined from the OI mapped travel time (τ) values and the GEMs, were averaged in 10-km-wide bins centered at 10-km intervals from the stream coordinates core. No vertical or horizontal smoothing was applied. The number of velocity observations averaged in each stream coordinates bin ranges from about 10 observation days for the bins 150 km from the core to about 300 observation days at the core. Only bins with at least 20 observation days were judged to have useful means, which restricted the usable range to bins centered at 90 km on the cold side of the SAF and at 120 km on the warm side of the front.

[13] The bottom depths at the seven HEFR sites within the main array ranged from about 3600 m to about 4300 m. As discussed by *Meinen et al.* [2002], to simplify the calculations all IES-based geostrophic velocities were determined relative to 4000 dbar. Absolute referencing of the geostrophic relative velocities was accomplished by interpolating or extrapolating to the actual pressure of the HEFR being used (errors introduced by this interpolation/extrapolation are negligible given the weak observed shears at these depths). The effect of the bottom depth on the stream coordinates averaging is complicated by the movement of the SAF over the bottom topography. A mean bottom depth for each 10-km stream coordinates bin was determined by averaging the bottom depths of the HEFRs based on the contribution of each HEFR to the velocities averaged in each bin. This mean bottom topography is included on all of the section plots shown in the paper and was used in the calculations of transport. Note that the bottom topography in the region is generally much more complex than is suggested by the mean topography in the figures.

4. Results

4.1. Direction of the Mean "Synoptic" SAF

[14] The stream coordinates mean absolute flow direction is 28° north of east (62°T), essentially the same as the Eulerian mean flow direction (relative to the bottom) of 30° north of east (60°T) found in the northern portion of the array (Figure 1). These directions are consistent with the mean currents observed by the AUSSAF moorings in 1993–1995 [*Phillips and Rintoul*, 2000]. The large-scale ACC flow direction is toward the southeast in this region, set by the large-scale topography between 140°E and 165°E. Maps of Z_6 on individual days clearly indicate a large amount of variability in the SAF direction (Figure 3); however, the presence of northeastward flow in a 4-year mean (AUSSAF and SAFDE combined) suggests the presence of a semipermanent standing meander at this location. Such a meander is not evident in the large-scale satellite study of *Gille* [1994] (see Figure 1) or in the large-scale hydrographic study of *Orsi et al.* [1995]. This either indicates long timescale changes between the time periods of those studies and the period encompassing AUSSAF and SAFDE, or a lack of spatial resolution in the two earlier large-scale studies. A recent compilation of surface drifter data in the Southern Ocean provides additional evidence for a time-mean standing meander at the location of the SAFDE (P. Niiler, personal communication, 2002), and such a meander is found in some numerical model simulations, for example, FRAM [see *Best et al.*, 1999, Figure 5].

4.2. Mean Synoptic Currents, Temperature, and Salinity of the SAF

[15] Figure 4 presents the mean along-stream absolute velocity along the SAF. Peak velocities of about 50 cm s^{-1} were observed at the surface, with 3500-dbar mean velocities of up to 2 cm s^{-1}. There is a suggestion of an equatorward shift of the velocity maximum with increasing depth; however, this shift is quite small compared to the observed shifts in midlatitude western boundary currents such as the Gulf Stream [e.g. *Johns et al.*, 1995]. The velocities are similar in magnitude to the SAF velocities observed in the Drake Passage from a series of CTD sections where the relative velocities were referenced by moored current meters [*Whitworth et al.*, 1982]. The standard deviation of our observed along-stream velocities (Figure 4c) demonstrates that the strength of the ACC flow along the SAF in our region changes significantly, with the core at the surface having a standard deviation of about 25 cm s^{-1}. Since the effect of meandering is removed from the stream coordinates reference frame, the baroclinic nature of the standard deviations indicates that the baroclinic

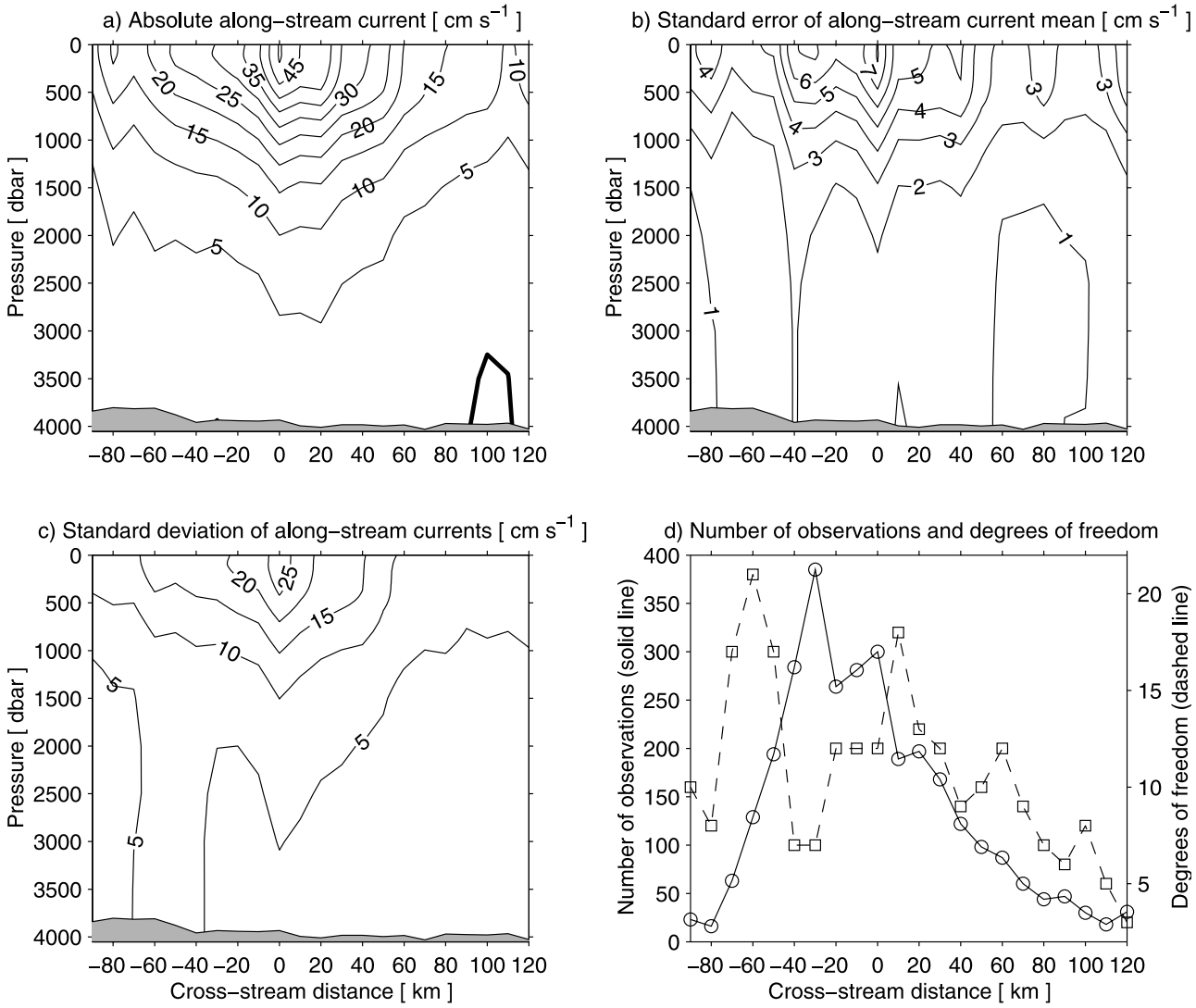

Figure 4. (a) Stream coordinates mean absolute current section calculated over the 701-day experiment. Current shown is the component along the stream path. (b) Standard error of the mean along-stream current. (c) Standard deviation of the along-stream current. (d) Number of observations used in developing the stream coordinates mean (solid line with circles) and the number of degrees of freedom obtained from the measurements (dashed line with squares; see Appendix A for explanation of calculation). Mean bottom topography (determined as weighted average of HEFR depths used in determining the current in each bin) is shown as shaded region in Figures 4a, 4b, and 4c. Actual bottom topography in this region is much more complex.

structure varied greatly during the experiment. On the basis of the estimated number of degrees of freedom (see Appendix A), the statistical standard error of the mean is also shown (Figure 4b), indicating that the velocity and structure presented are quite robust with uncertainties of only 5–7 cm s^{-1}.

[16] The cross-stream mean absolute velocities (Figure 5a) exhibit a strong horizontal diffluence at the SAF southwest of Tasmania. The cross-stream velocity diffluence has strong baroclinic (relative to the bottom) and weak barotropic (bottom velocity) components. The strong baroclinic cross-stream diffluence is unexpected; diffluence and confluence patterns around the Gulf Stream, which is generally viewed as the archetype for strong ocean currents, are believed to be mainly barotropic [e.g., *Hogg*, 1992]. The statistical standard error of the mean cross-stream flow (Figure 5b) indicates that the SAF cross-stream diffluence pattern is statistically significant up to the 95% confidence level (albeit only just). The SAF diffluence in Figure 5a contradicts results from earlier surface drifter studies wherein drifters were deployed at a wide range of longitudes along the length of the SAF. The drifters indicated that the entire length of the SAF was a region of horizontal flow confluence near the surface [*Hofmann*, 1985]. However, recent analyses of the WOCE SR3 hydrography [*Rintoul and Sokolov*, 2001] southwest of Tasmania imply a loss of SAF transport to the north, as part of a baroclinic recirculation, consistent with the northward flow on the north side

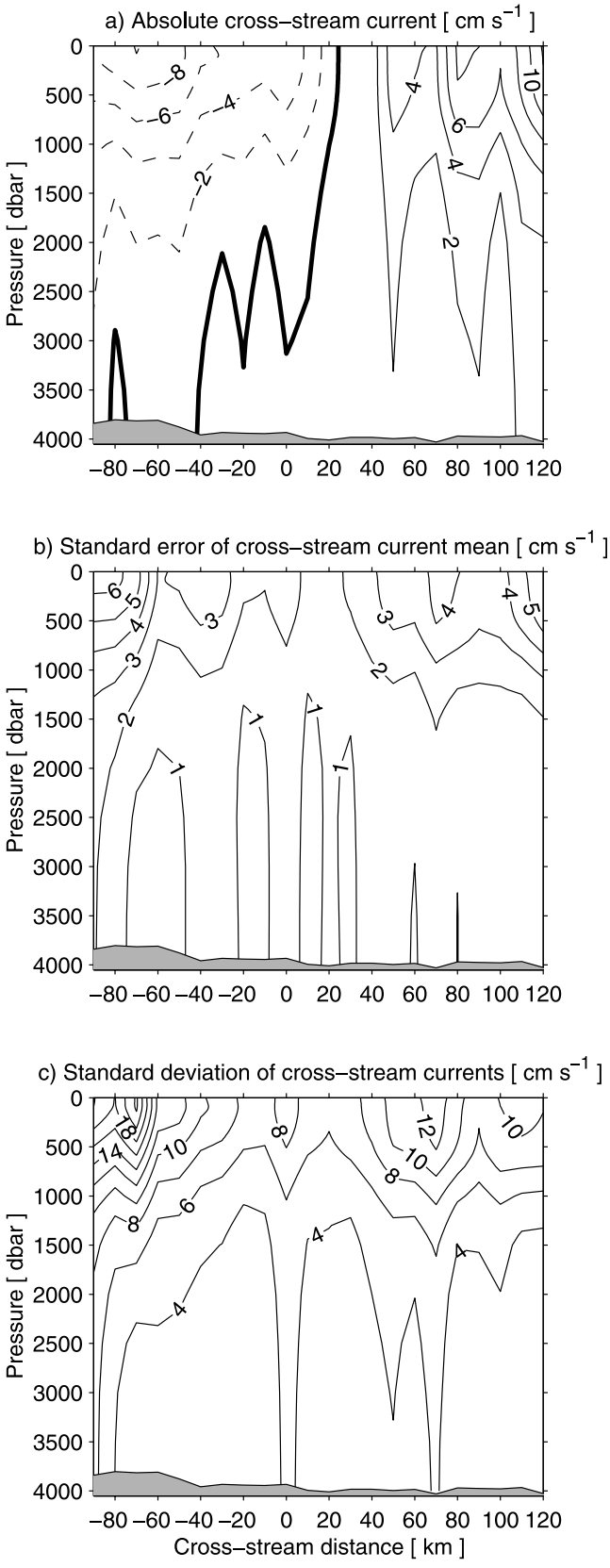

Figure 5. Same as Figures 4a–4c but for the component of velocity perpendicular to the stream path.

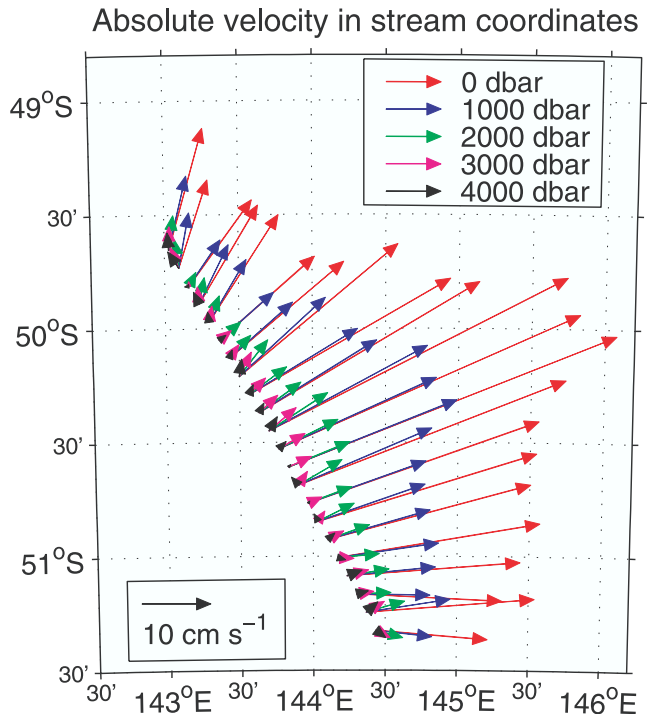

Figure 6. Stream coordinates mean absolute velocities at the five pressure levels indicated in the legend. The location of the SAF was chosen based on the time mean location of the core (50.6°S) along the HEFR line; the direction of the core flow was based on the time mean downstream direction from the OI mapped Z_6 fields.

of the SAF in Figure 5a. The southward diffluence in Figure 5a may be partially due to the southern current indicated in Figure 1; however, when the mean velocity sections were recalculated without using time periods when a second front was clearly identifiable within the array (which tossed out about 25% of the observations), the maximum resulting reduction in the southward flow on the cold side of the SAF was 2 cm s^{-1}. The changes were not statistically significant at the 95% level, indicating that the southward flow away from the SAF core is a robust result. The implications of these diffluence observations for vertical velocity will be discussed in a future paper.

[17] Figure 6 presents the mean stream coordinates velocities in plan view, where the core is placed at the time-mean location where it crosses the HEFR line; the core direction is given by the time-mean downstream direction from the OI mapped Z_6 fields, and the vectors are plotted along a line perpendicular to the time-mean core direction. The diffluence of the cross-stream flow is visually obvious, as is a small amount of backing and veering with height. Because the GEM method forces the baroclinic velocities to be parallel in the vertical, the backing and veering is due solely to the barotropic contribution from the HEFR measured absolute velocities.

[18] Mean stream coordinates temperature and salinity sections (Figure 7) were determined using the same methodology as for the velocity sections described earlier. The temperature section displays a thermostad layer between 8°C and 9°C on the warm (north) side of the front. The

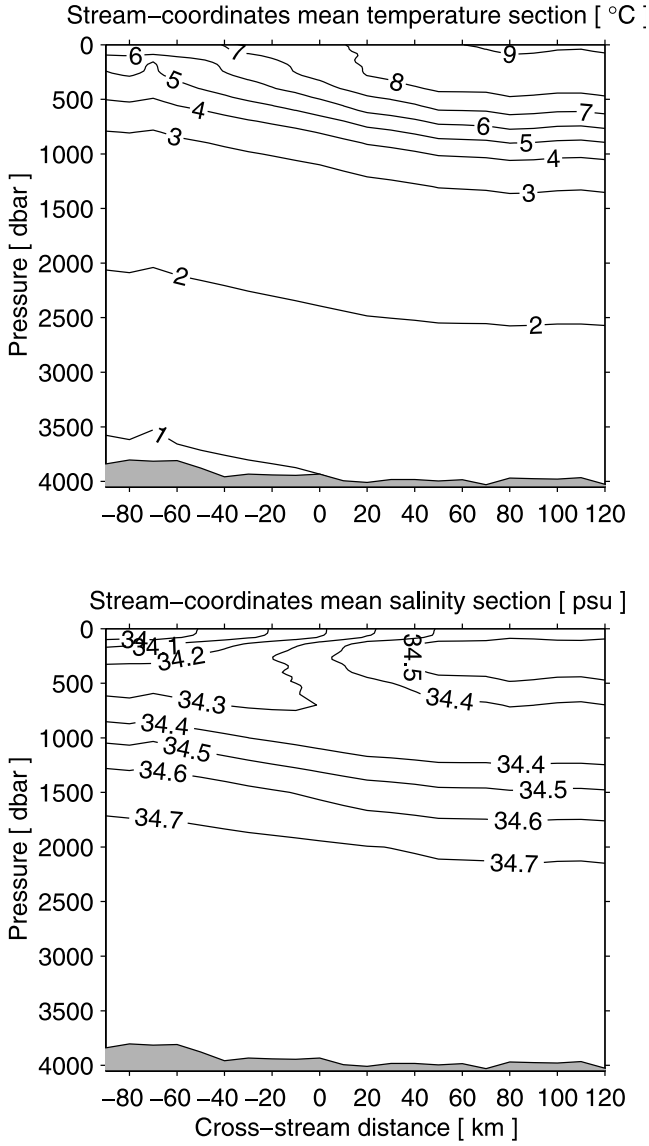

Figure 7. Stream coordinates mean temperature and salinity sections.

thermocline depth (approximated by the 6°C isotherm depth) changed by roughly 700 dbar across the front. The salinity section shows a halostad of 34.5 psu to the north of the core overlying a salinity minimum layer between 750 dbar and 1250 dbar. The salinities within this minimum layer, 34.3–34.4 psu, are consistent with Antarctic Intermediate Water, while the salinities within the halostad are within the commonly observed range for Subantarctic Mode Water in this region [*Tomczak and Godfrey*, 1994; *Hanawa and Talley*, 2001].

[19] The accuracy of the velocities and temperatures shown in these figures is dependent upon the measurement accuracy of the various instruments as well as the accuracy of the interpretation methods (such as the GEM technique). The details of the error analyses are left to Appendix A; in brief, combining measurement accuracy, methodological accuracy, and statistical accuracy, the mean absolute velocities near the core of the SAF have accuracies ranging from 7 cm s^{-1} near the surface to 1 cm s^{-1} at depth. Below the upper 100–200 dbar, where seasonal variability is large, the mean temperatures (salinities) within the main thermocline (halocline) are accurate to within 0.1°C (0.02 psu); below 2000 dbar the accuracy improves to 0.015°C (0.001 psu).

4.3. Horizontal Structure of Along-Stream Velocity

[20] Figure 8 presents a comparison of the along-stream velocities obtained in SAFDE and those obtained by *Phillips and Rintoul* [2002], hereinafter referred to as PR02, from an analysis of up to 2 years of current meter data from the four AUSSAF mooring locations in 1993–1995. Velocities are shown for the 420 dbar, 1150 dbar, and 3320 dbar levels; comparisons at the two other depths (780 dbar and 2240 dbar) available in PR02 are similar. Note that PR02 used a slightly modified version of the *Hall and Bryden* [1985] and *Hall* [1986] method for determining stream coordinates, incorporating the "frozen field" and "vertical shear" methods discussed earlier, while this study used the OI methods recommended by ML03. The two studies also used different definitions for the origin of the cross-stream distance axis. In order to compare the velocity cross-sections, the offset between the median location of strong flow for the two studies was determined ($\geq$20 cm s^{-1} for this study and $\geq$30 cm s^{-1} for PR02), and the PR02 cross-sections were shifted by the amount of the offset (about 11 km).

[21] The velocity cross-sections shown in Figure 8 differ in three ways: the flow strength, the presence or absence of secondary peaks, and the current width. The flow observed by PR02 is stronger than the flow observed during SAFDE, both near the core and at the flanks (Figure 8). These differences generally exceed the combined error bars of the SAFDE section (see Appendix A) and PR02 (see their Figure 6). There are a number of possible reasons for the differences. First, the current meters used by PR02 should observe stronger core velocities because they are point measurements, while the SAFDE velocity measurements are based on HEFR measurements (which intrinsically represent an average over a horizontal circle with a radius equal to the water depth [*Chave and Luther*, 1990]) and geostrophic velocities determined from neighboring IES measurements (which represent the horizontal average across the gap between the IESs, in this study roughly 30 km). Second, there could be real interannual changes between the 1993–1995 period of the PR02 observations and the SAFDE 1995–1997 period. Third, there are differences in how the stream coordinates representations were derived.

[22] By applying both the frozen field-vertical shear methods and alternately the OI method to the same data set, ML03 demonstrate the resulting mean current strength depends on the stream coordinates method chosen. They found that the vertical shear method leads to stronger along-stream flows, particularly along the flanks, because any diffluent baroclinic cross-stream flow (Figures 5 and 6) is rotated into the along-stream component by this technique. *Bower and Hogg* [1996] document further concerns about using the vertical shear method in the presence of a curved current path. The use of the frozen field assumption, i.e., a time-invariant cross-stream structure as described earlier, also contributes to a stronger along-stream velocity, partic-

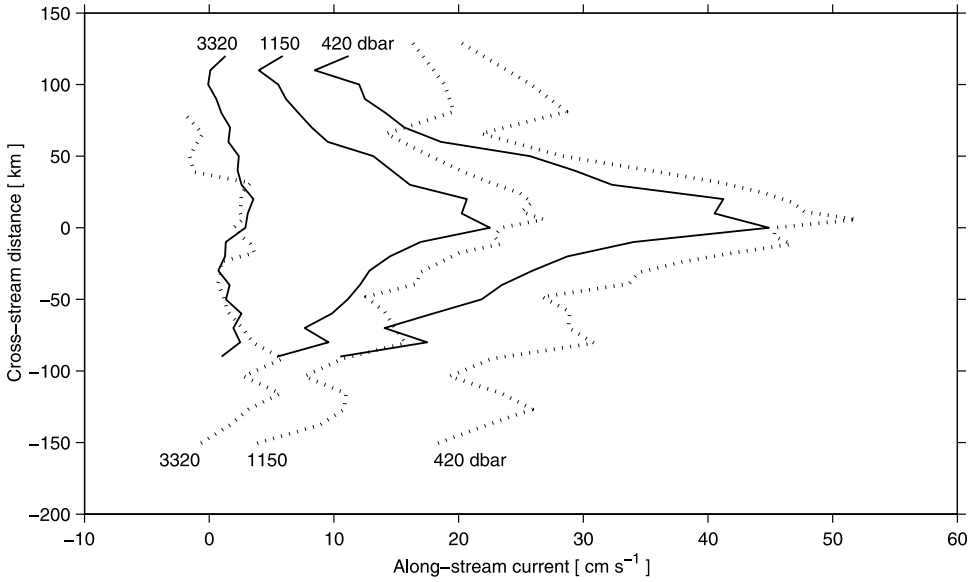

Figure 8. Comparison between the SAFDE stream coordinates mean along stream currents at three pressure levels versus the currents determined by *Phillips and Rintoul* [2002]. Pressure levels are as noted in the figure; solid lines denote SAFDE results while dotted lines denote the results from *Phillips and Rintoul* [2002].

ularly along the flanks of the current, when compared to the OI method. Sufficient data do not exist to definitively state whether the different time period, the different measurement types (point moorings versus mapped IES data and HEFR data), or the different stream coordinates analysis methods account for most of the observed differences in mean along-stream velocity shown in Figure 8. However, the results of ML03 clearly indicate that stream coordinates methodology differences play a significant role.

4.4. Multiple Branches to the SAF?

[23] A remarkable difference between the ACC and other strong oceanic flows such as western boundary currents is the bandedness of the ACC, with part flowing along the SAF and part flowing along the PF as well as some smaller contributions from one or more additional fronts [e.g., *Rintoul et al.*, 2001]. This multiple front structure for the ACC is commonly called "zonation," and the strongest three fronts are believed by most researchers to be contiguous around the globe [*Hofmann*, 1985; *Gille*, 1994; *Orsi et al.*, 1995], although the fronts may merge at some longitudes [e.g., *Rintoul et al.*, 2001]. Several studies incorporating data from CTD and XBT sections, along with satellite altimetry, have suggested that the SAF and PF may both be further broken into two or three fronts (with associated currents) at various points around the globe [*Read et al.*, 1995; *Sokolov and Rintoul*, 2002]. The Eulerian mean vertically averaged relative velocities shown in Figure 1 clearly indicate two separate velocity peaks with the flow at the northern instrument sites trending northeast, while the flow at the southern instruments tended toward the east-southeast with a relative minimum between these flows.

[24] PR02 suggest that the additional peaks observed in their cross-stream sections (reproduced in Figure 8) may represent additional branches of the SAF. However, their local peaks and valleys do not differ by more than their error bars, and hence their analysis would also be consistent with a monotonic decrease on each flank. Our velocity profiles across the same levels are smoother, which may reflect more degrees of freedom from our mapping observations. Nevertheless, the lack of secondary peaks in the SAFDE analysis of the SAF indicates that the additional peaks are not robust features of the circulation in this location.

4.5. SAF Current Width

[25] An important characteristic of any oceanic current is its width. As shown in Figure 8, the SAFDE and PR02 cross-sections span significantly different ranges. The stream coordinates method applied by PR02 does not actually use a direct measurement of cross-stream location, inferring it instead using temperature measurements from a mooring and the "frozen" cross-stream structure relationship. This assumption may contribute to the increased width of the PR02 velocity cross-section shown in Figure 8. If the SAF width is defined as the distance between the points where the along-stream surface velocity reaches 50% of its peak value, the SAFDE results indicate the mean SAF is about 100 km wide at the surface (Figure 4). If instead the width is defined as the distance between the zero along-stream velocity points, the SAF is roughly 290 km wide at the surface (this estimate requires extrapolating our velocities outward a small amount as our cross-section was not quite wide enough to reach zero crossings). This zero-to-zero width is a bit smaller than the global mean SAF width determined from altimetry data by *Gille* [1994], estimated as about 325 km based on her mean Gaussian width and her Figure 3. On the other hand, the SAFDE widths are much larger than the 50–60 km estimated widths of the fronts in the Drake Passage, chosen subjectively on the basis of watermass transitions from a series of vertical property sections from CTDs and XBTs [*Nowlin and Clifford*,

1982]. Snapshot cross-sections of the SAF have also been made at other locations around the globe, such as at the Greenwich Meridian [*Whitworth and Nowlin*, 1987] and along several WOCE lines in the south Pacific sector [*Donohue et al.*, 2001]. These studies, however, have been based on small numbers of CTD sections. A well-known problem for current structures derived from CTD sections is that although these sections can produce an accurate estimate for the transport of the current, the velocity estimates may appear artificially low and the current may appear artificially wide because the section may be crossing the current obliquely. Furthermore, the CTD-section-based methods represent only a single snapshot in time, whereas the stream coordinates section presented here represents a time mean over roughly 2 years. Because significant variability of the temperature front width has been documented in the SAF using the IES array data from SAFDE (ML03), the snapshot technique may not provide a particularly useful measure of the structure or width of the SAF.

[26] For comparison with the SAF width estimates from the SAFDE data, consider the time-mean velocity structure of the Gulf Stream which was obtained during the SYNOP experiment [*Johns et al.*, 1995]. Near 68°W, 37°N, the Gulf Stream is significantly narrower by both of the above width measures, with corresponding widths of about 60 km and 180 km, respectively, for the 50% velocity and zero velocity cutoffs. At first glance this difference in widths, with the SAF being much wider than the Gulf Stream, is somewhat counterintuitive because simple models of oceanic inertial jets [e.g., *Fofonoff and Hall*, 1983] have widths scaling like the internal Rossby radius, which decreases toward the poles. Also, some altimetry studies have indicated that the horizontal scales of ocean variability tend to correlate well with the internal Rossby radius of deformation [e.g., *Stammer*, 1997]. Recent modeling studies, however, indicate that the mean scale of the ACC fronts is set by a combination of the β effect, eddy-mean flow interaction, and the bottom topography, not the internal Rossby radius [*Treguier and Panetta*, 1994; *Sinha and Richards*, 1999]. The altimeter study of *Gille* [1994] also indicated that the dependence of the SAF width on internal Rossby radius was weak, accounting for less than 7% of the total variance in SAF width around the globe. The SAF width estimated from the SAFDE data will provide a benchmark for testing models of the ACC circulation [e.g., *Treguier and Panetta*, 1994; *Grose et al.*, 1995; *Best et al.*, 1999; *Sinha and Richards*, 1999].

4.6. Baroclinic Versus Barotropic Velocities

[27] Most previous studies of the ACC have been limited to determining baroclinic velocities from hydrography, and as such those velocities are relative to an assumed level of no motion. The SAFDE study provides an opportunity to quantify the error in that assumption, and hence the magnitude of the barotropic (bottom velocity) components. Figure 9 shows the along-stream and cross-stream velocities relative to a level of no motion at the bottom. The differences between these sections and the corresponding absolute velocity sections (Figures 4a and 5a) can be represented by line plots (Figures 9c and 9d), rather than sections, because the differences are depth-invariant in nature. Since this paper focuses on the time-mean results, the differences that are shown here represent the mean barotropic (bottom velocity) flows. The along-stream barotropic flow was mainly positive across the section, with along-stream peak values of 1.5–2 cm s^{-1} and peak counterflows of less than 0.5 cm s^{-1}. None of these barotropic velocities are statistically different from zero (Figure 4b). The effect of the along-stream barotropic flow is to shift the core of the flow slightly equatorward, although the magnitudes of the bottom velocities are so small as to make the shift negligible. The cross-stream barotropic flow is generally northward across nearly the entire cross-section, peaking near 2 cm s^{-1} north of the core and reducing to near zero south of the core (only the largest values are statistically significant). The barotropic cross-stream flow shifts the location of the center of the upper ocean diffluence and brings the peak positive and negative cross-stream magnitudes closer to equal at similar distances from the core on both sides. Other than these effects, the mean relative velocity structure was very similar to the mean absolute velocity structure. This was not true for the time-varying signal, however, because the observed near-bottom velocities at times exceeded 10 cm s^{-1} for periods of several weeks (e.g., Figure 2).

4.7. Cross-Stream Gradient of Along-Stream Velocity

[28] Simple analytical models of an inertial jet imply that the cross-stream gradient of the along-stream velocity should have a larger magnitude on the cold side of the current [*Fofonoff and Hall*, 1983; *Hall*, 1986]. This characteristic is also reproduced in high-resolution numerical models of oceanic jets that have separated from the continental boundary, although the asymmetry diminishes somewhat with distance from the boundary (e.g., the Gulf Stream in the *Smith et al.* [2000] model of the North Atlantic). *Johns et al.* [1995], employing a large array of instruments and a stream coordinates method similar to our mapping method, found the strongest horizontal shear magnitude on the cold side of the Gulf Stream in accordance with theory. Subsequent observations from repeat shipboard acoustic Doppler current profiler (ADCP) measurements have confirmed a stronger gradient magnitude on the north (cold) side of the Gulf Stream [*Rossby and Zhang*, 2001]. On the basis of the stream coordinates mean section of Figure 4, the SAF also displays slightly stronger horizontal shear magnitude on the cold side (if the frozen field and vertical shear type of stream coordinates are applied to the SAFDE data, the result is a stronger cross-stream gradient magnitude on the warm side of the front (ML03)). The weakness of the asymmetry is consistent with the absence of a continental boundary upstream of the SAFDE site and the generally zonal nature of the ACC flow. The weak asymmetry is also consistent with the relatively small (10%) change of the first internal Rossby radius across the SAF [see *Rossby and Zhang*, 2001].

4.8. Vertical Structure Within the SAF

[29] As noted earlier, the vertical structure estimated from the SAFDE data results from an empirical mode, the GEM, and not the dynamical normal modes [e.g., *Philander*, 1978]. Other authors have analyzed ACC velocity measurements in terms of the dynamical normal modes [e.g., *Inoue*, 1985; *Sun and Watts*, 2001]. Since the GEM approach also

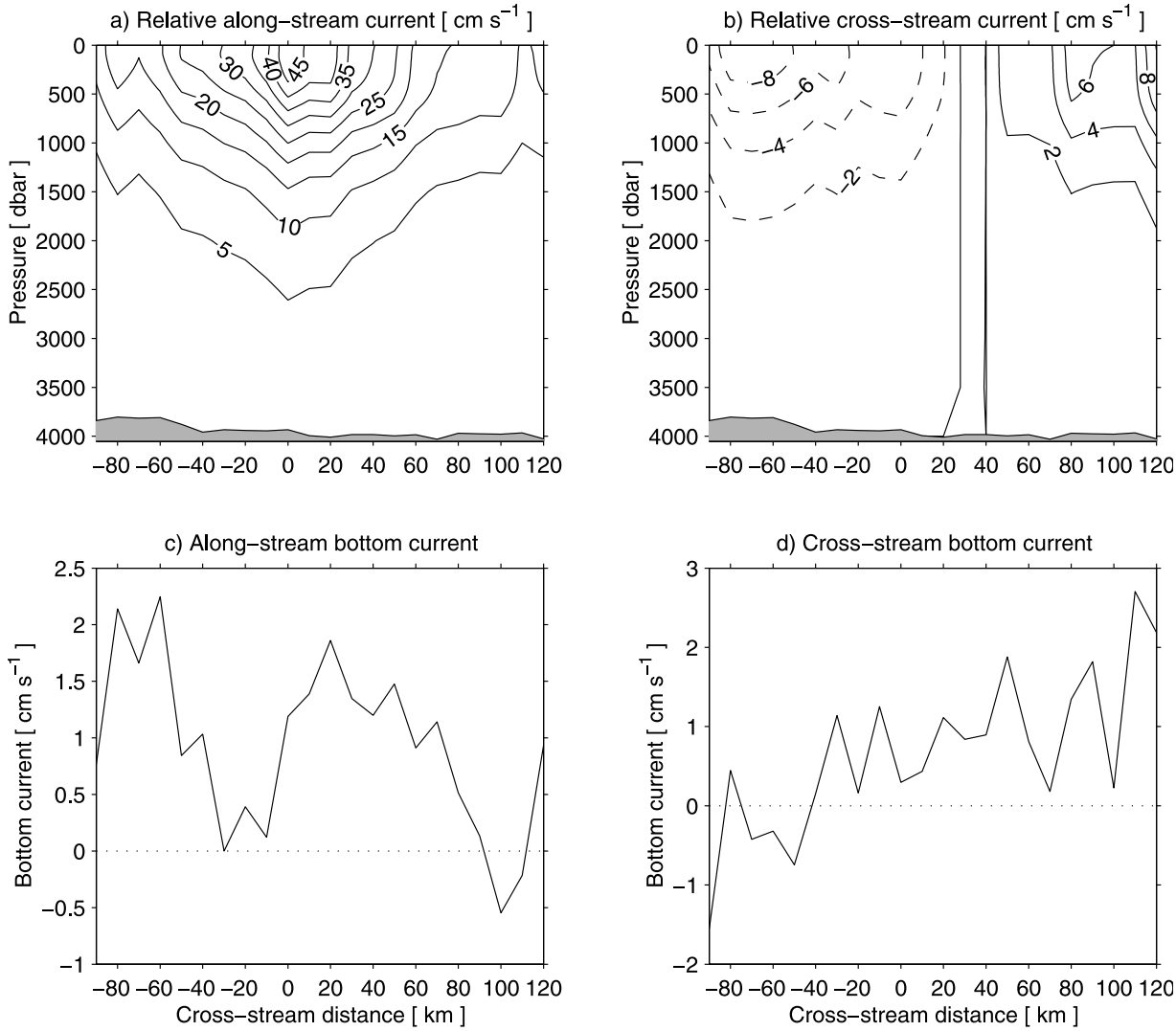

Figure 9. (a) Stream coordinates mean along-stream current relative to a level of no motion at the bottom. (b) Stream coordinates mean cross-stream current relative to the bottom. (c) Along-stream component of the barotropic (bottom) velocity. (d) Cross-stream barotropic (bottom) velocity. Mean bottom depth indicated in Figures 9a and 9b by shaded regions.

provides temperature and salinity estimates, dynamical normal modes can be calculated and compared with the observed GEM vertical structure.

[30] The temperature and salinity profiles at −40 km, 0 km, and +40 km were extracted from the stream coordinates mean sections illustrated in Figure 7 and were used to calculate the buoyancy frequency, N, for each location. The dynamical normal modes were then calculated for each of the three N profiles and are shown in Figures 10–12. These modes are sometimes referred to as the barotropic and baroclinic modes; however, this terminology can be confusing in light of the Fofonoff definitions of barotropic (bottom velocity multiplied by depth) and baroclinic (relative to bottom) transport which are being used in this paper. For this reason the normal modes will be referred to as the external (depth invariant) mode and the internal (depth varying) modes.

[31] The first four modes for the −40 km N profile, from the cold side of the SAF, are illustrated in Figure 10. The modes at the core (Figure 11) are very similar in structure to those at −40 km; however, there is some vertical offset of the location of the maximum vertical gradients. The modes at +40 km on the warm side of the SAF (Figure 12) are also similar in vertical structure to those on the cold side and at the core, however the vertical offsets are even larger with the modal peaks and peak gradients occurring 100–300 m deeper on the warm side of the SAF than on the cold side. This change in depth is consistent with the deepening of the main thermocline (pycnocline) across the SAF. Aside from the change in depth of the mode peaks and maximum gradients, the structures of the normal modes are very similar across the SAF.

[32] As discussed earlier, SAFDE provides the opportunity to test how well the normal modes match the observed velocity structure. A key advantage of using the SAFDE data sets for this comparison is that the combination of HEFR measurements, IES measurements, and the GEM method provides a full water column profile of velocity

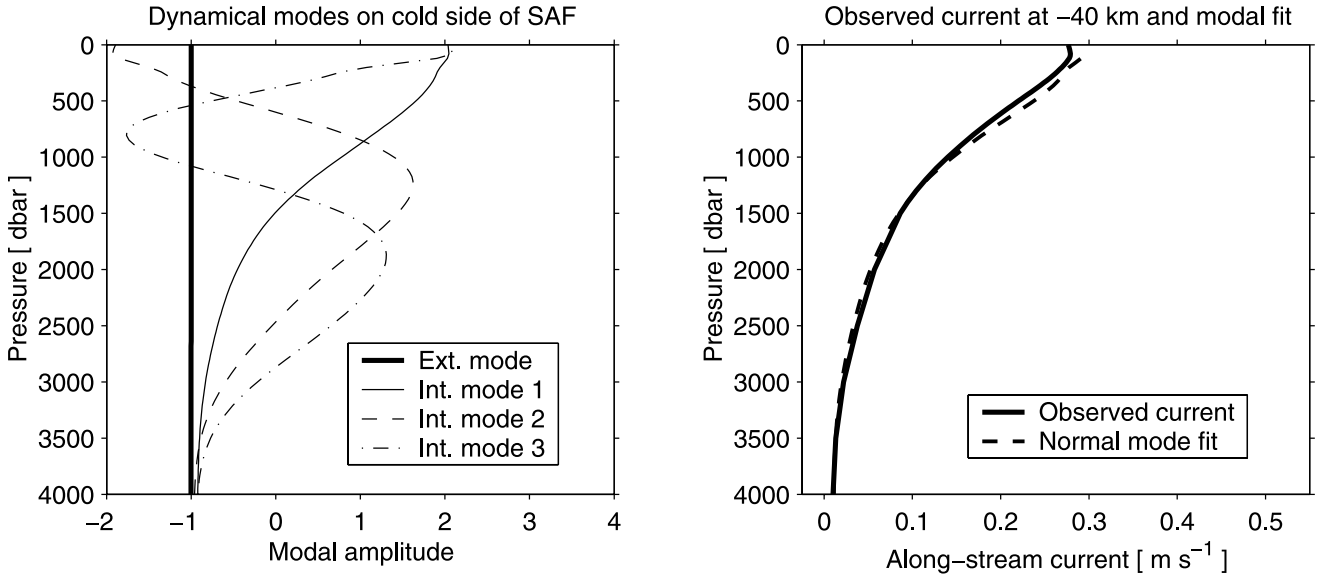

Figure 10. (left) First four normal modes derived using the N profile calculated from the stream coordinates mean temperature and salinity profiles at −40 km along the cross-stream axis. The external and internal modes are identified by the legend. (right) Observed stream coordinates mean along-stream current at −40 km along the cross-stream axis as well as the normal mode fit from a summation of the external and first three internal modes.

for comparison with the normal mode structure. Most previous studies have been limited to using velocity observations at only a small number of depths from current meters on a mooring [e.g., *Inoue*, 1985]. Figures 10–12 illustrate the observed stream coordinates mean along-stream velocity at −40 km, 0 km, and +40 km, respectively. Also shown are the least squares normal mode fits to the observed profiles using the external and first three internal modes. The values of the surface current associated with each of the modes at the ocean surface are shown in Table 1. The surface values show the minimal impact of the second and third internal modes at all three locations across the SAF. At deeper levels the higher modes play a similarly small role. The dominance of the external and first internal mode in accounting for the vertical structure of the currents is consistent with *Inoue*'s [1985] analysis of currents obtained from moorings in the Drake Passage, but contradicts the conclusion of *Sun and Watts* [2001] that the derived geostrophic current structure in the Southern Ocean (using a similar GEM methodology) differs greatly from the structure of the calculated first internal mode. The latter made the mistake of using a 3000 m depth in calculating the

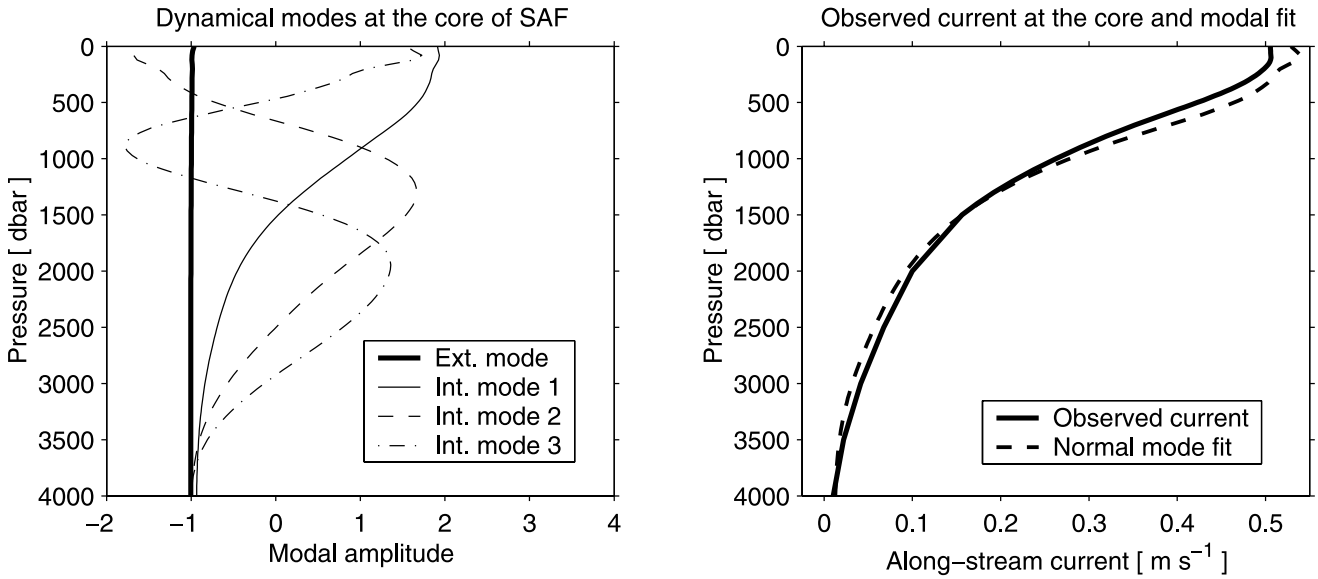

Figure 11. Same as Figure 10 except at 0 km along the cross-stream axis.

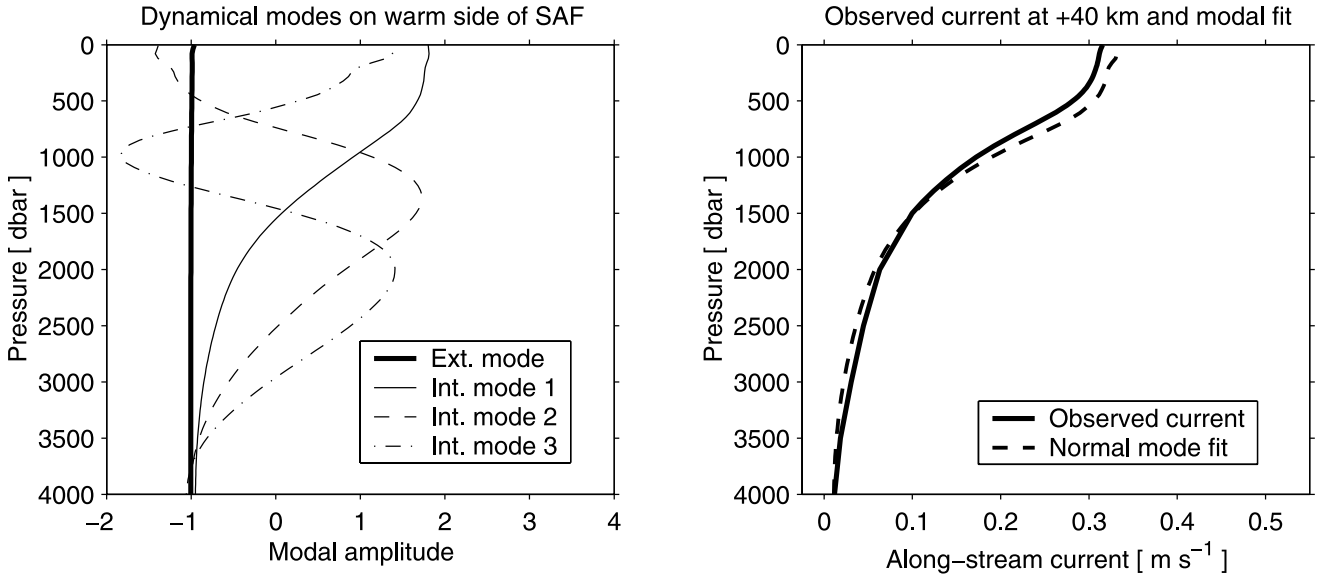

Figure 12. Same as Figure 10 except at +40 km along the cross-stream axis.

internal modes in a region where significant vertical shear extends to the bottom (near 4000 m). This artificially suppressed the deep velocities and vertical shear compared to the observed structure in those depths.

[33] While the observed vertical structure is quite similar to that of the mode fit, there are significant differences. At all three cross-stream locations, the vertical gradient of along-stream velocity is larger below 2000–2500 m in the observations than in the mode fit, while between 700 m and 2000 m the vertical gradient is larger in the mode fit than in the observations. The correspondence between modes and observations is best at −40 km and worst at 0 km. Of course, the dynamical normal modes are explicitly valid only for a flat bottom and horizontally uniform stratification, which are inappropriate assumptions in the SAFDE region (see Figures 1 and 7). With these caveats in mind, the vertical structure obtained from the GEM method corresponds primarily to a combination of the external and first internal modes with only small contributions from the higher internal modes.

4.9. Relative and Potential Vorticity

[34] Relative vorticity is determined from the following equation:

$$\zeta = \frac{\partial v}{\partial x} - \frac{\partial u}{\partial y}, \tag{1}$$

where (u, v) and (x, y) are, respectively, the velocity components and the unit vectors in the zonal and meridional directions. The coordinate system can be rotated into any horizontal direction without changing the equation, so if we rotate the coordinates such that x and u refer to along-stream direction and velocity, respectively, then the two terms in equation (1) become the along-stream gradient of cross-stream velocity and the cross-stream gradient of along-stream velocity. The latter term can be determined from the section shown in Figure 4. Scaling analysis suggests that the along-stream gradient of cross-stream velocity should be small in comparison to the cross-stream gradient of along-stream velocity. Unfortunately, a single mean cross-stream section such as Figure 5 does not provide the means to test this hypothesis. However, as *Cushman-Roisin* [1994] demonstrates, the relative vorticity can be determined as

$$\zeta = \frac{\partial V}{\partial n} - \kappa V, \tag{2}$$

where $V = (u^2 + v^2)^{1/2}$ is the flow speed, n is the cross-stream distance measured positive to the right of the flow, and κ is the path curvature. Because our velocity measurements have already been rotated into stream coordinates, the first term on the right side of equation (2) is easily calculated. For κ, *Watts et al.* [1995] showed that path curvature for the baroclinic front can be estimated by determining the spatial gradients of an OI field of the depth of a particular isotherm which occurs in the center of the main thermocline. *Watts et al.* [1995] used the depth of the 12°C isotherm, Z_{12}, in the Gulf Stream for this purpose; for the SAF the 6°C isotherm depth, Z_6 was employed. Following the *Watts et al.* [1995] method, the curvature was determined at each OI grid point within the IES array on each day. The values of curvature along the $Z_6 = 500$ dbar line were extracted. The median of the resulting curvature estimates on each day was substituted into equation (2) to obtain an estimate for the stream coordinates mean relative vorticity (Figure 13, top panel). There is a stronger relative

Table 1. Surface Current Associated With Each of the Dynamic (Normal) Modes at Three Sites Spanning the SAF[a]

	External Mode	Internal Mode 1	Internal Mode 2	Internal Mode 3
Cold side (−40 km)	+9	+18	+1	< +1
SAF core (0 km)	+16	+33	+2	+1
Warm side (+40 km)	+11	+20	+1	< +1

[a]Values are in cm s^{-1}.

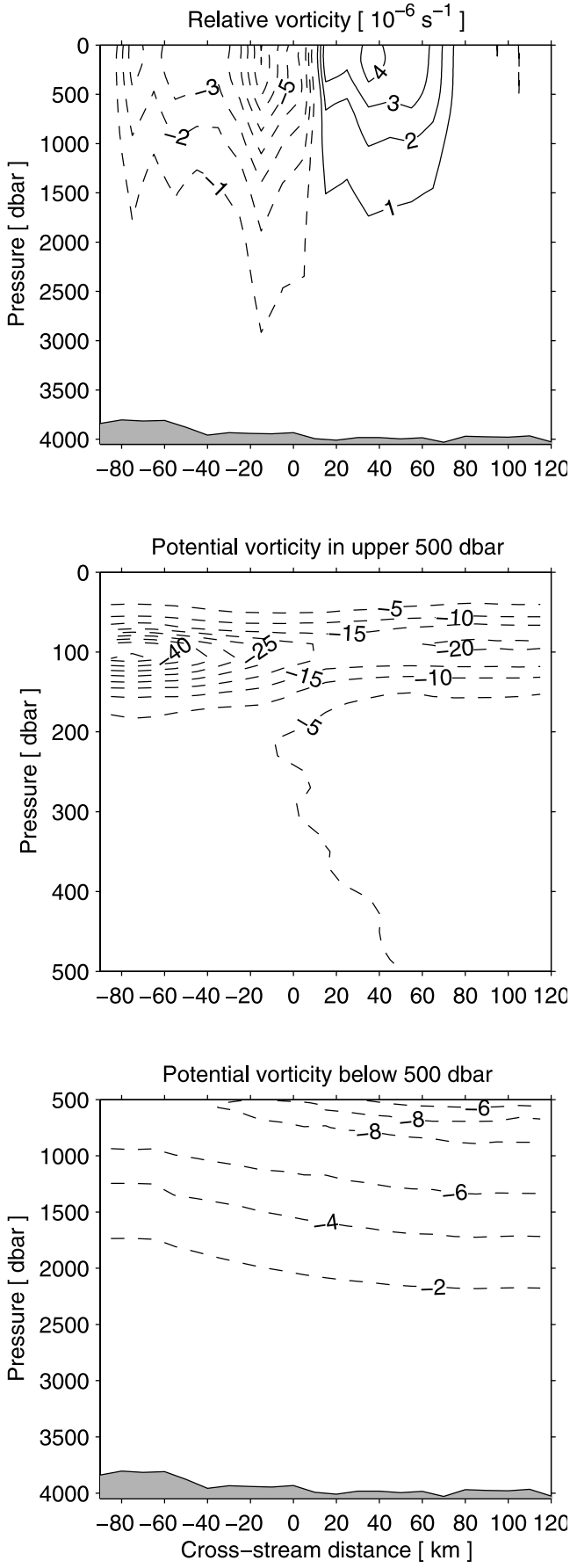

vorticity magnitude on the cold side than on the warm side, with magnitudes as much as 100% higher over most of the water column. An important additional fact is that the planetary vorticity ($|f| = 1.1 \times 10^{-4}$ s^{-1} at 51°S) is much larger than the observed relative vorticity, so the effect of ζ on the total vorticity is quite small.

[35] The stream coordinates mean temperature and salinity sections (Figure 7) were combined to calculate a mean potential density section (not shown). The vertical gradient of potential density was then combined with the relative and planetary vorticities to estimate a stream coordinates mean potential vorticity (PV) section (Figure 13, middle and bottom panels). Potential vorticity is given by

$$PV = -\frac{1}{\rho_o}\frac{\partial \sigma_\theta}{\partial z}(f + \zeta), \tag{3}$$

where σ_θ is the potential density and z is the vertical coordinate. Figure 13 reveals a thin (≈150 dbar) shallow (≈100 m deep) layer of high PV on the cold side of the SAF. On the warm side of the SAF, there is a similar (≈120 dbar) layer of moderately high PV, although the peak values on the warm side are only 50% of the peak values on the cold side. Between 500 and 1000 dbar, there is an additional thin relative maximum layer on the warm side of the SAF. Because relative vorticity is so much smaller than the planetary vorticity ($\zeta < 0.1 \times f$), the differences in PV across the front are due primarily to density gradient differences across the front. This potential vorticity section will be used in a future paper in a discussion of the stability and energetics of the SAF.

4.10. Transport Along and Across the SAF

[36] Vertically integrating the along-stream velocity section and multiplying by the width of each horizontal bin yields an estimate of the absolute transport which flows along the SAF. The total absolute transport along the SAF integrated over the 10-km-wide bins centered from −90 km to 120 km (a total width of 220 km) was 75 Sv (Sv = 10^6 m^3 s^{-1}). This transport is somewhat lower than had been expected. *Rintoul and Sokolov* [2001], employing six WOCE CTD sections at roughly the same geographic location as SAFDE, estimate the baroclinic transport of the mean SAF to be 105 Sv (using a width of roughly 300–400 km), while *Yaremchuk et al.* [2001], using the same section data in an inverse model, found a mean transport of 110 Sv (although this latter estimate spanned an integration range of about 700–750 km and also included an indeterminate portion of the PF transport). The 75 Sv

Figure 13. (opposite) (top) Relative vorticity of the stream coordinates mean, calculated as described in the text. Units are 10^{-6} s^{-1}. (middle) Stream coordinates mean potential vorticity in the upper 500 dbar. (bottom) Potential vorticity below 500 dbar; note the contour interval change. Potential vorticity units are 10^{-11} m^{-1} s^{-1}. The relative vorticity has been calculated after a 30-km smoothing of the velocity sections to reduce the noise; no further smoothing was done for the potential vorticity sections. In all panels, solid contours indicate positive values, and dashed contours indicate negative values.

Table 2. Transport of the SAF From This and Other Studies[a]

	Estimated Width of SAF	Depth of Integration	Transport Within Domain	Barotropic Transport Contribution	Estimated Transport Without Metho dology Bias
		Stream Coordinates Estimates			
PR02	280 km	3800 m fixed depth	116 Sv	16 Sv	93 Sv
PR02 subsampled	220 km	3800 m fixed depth	92 Sv	13 Sv	73 Sv
SAFDE (this study)	220 km	variable bottom depth	75 Sv	8 Sv	–
		Eulerian (*Snapshot*) *Estimates*			
Nowlin Clifford [1982]	51 km	2500 m fixed depth	28 Sv	0 Sv	–
Donohue et al. [2001]	50–250 km	variable bottom depth	64 Sv	19 Sv	–
Rintoul Sokolov [2002]	300–400 km	variable bottom depth	105 Sv	0 Sv	–
Yaremchuk et al. [2001]	700 km	variable bottom depth	110 Sv	?Sv	–

[a]Second row of numbers gives results for the PR02 [*Phillips and Rintoul*, 2002] section integrated over a narrower range using their Figure 14. Fourth column gives the absolute transport. Fifth column lists the barotropic transport contribution (defined as bottom velocity multiplied by the water depth and current width). The final column lists the PR02 transport adjusted for the stream coordinates methodology differences (see text). The stream coordinates sections both used the maximum range of observations for determining the current width; Eulerian snapshots all used property criterion to define the boundaries of the SAF. Sections without absolute geostrophic reference velocities are listed as having zero barotropic contribution, while studies which did not break down the transport between barotropic and baroclinic contributions are listed with a question mark for the barotropic contribution. See text for locations of these studies.

SAFDE transport value (determined over the maximum possible range of 220 km) is also significantly smaller than the 116 Sv SAF stream coordinates absolute transport estimate (integration width 280 km) of PR02 at the same location as SAFDE but during 1993–1995. A number of issues contribute to these differences, some of which are illustrated in Table 2. The most basic contribution to the differences is the horizontal range over which the transports are integrated. For example, when integrated over a 220-km span similar to our estimate, the PR02 section yields a transport of 92 Sv, much closer to our 75-Sv estimate. Clearly, estimates of transport along such fronts as the SAF need to be accompanied by definitions of frontal width.

[37] Another contributor to the differences in Table 2 is methodology. ML03 obtained two different estimates for the mean stream coordinates structure of the flow along the SAF, using the same IES+HEFR absolute velocities for both but applying alternately the mapped IES stream coordinates method that leads to Figure 4 or a stream coordinates method similar to *Hall* [1986] and PR02. The velocity section derived from the latter method, when integrated over the same 220-km cross-stream range as the mapped IES method (which yielded 75 Sv), resulted in a transport of 94 Sv. When integrated over the wider 280-km range used by PR02, the transport increased to about 117 Sv, very similar to PR02's 116 Sv for their mooring data. On the basis of the ratio of the two ML03 transport estimates for the 220-km span, it is suspected that had PR02 been able to use the IES mapping technique for their stream coordinates, they would have observed a transport of 73 Sv in the 220-km integration and 93 Sv in the 280-km integration. Both numbers are significantly closer to the SAFDE estimate of 75 Sv, suggesting that the majority of the difference between the PR02 SAF transport estimate and the SAFDE transport estimate can be explained solely by methodological differences, although it is possible that other factors such as interannual variability may also be important.

4.11. Barotropic Versus Baroclinic Transport

[38] As illustrated in Table 2, the barotropic component of the transport (defined as the horizontal integration of bottom velocity multiplied by the water depth) represents only a small fraction of the SAFDE mean SAF transport estimate. The SAFDE barotropic component is much smaller than that observed by PR02, which itself is small relative to observations at other locations. *Donohue et al.* [2001] found that the barotropic component represented on average about 30% of the absolute transport of the SAF from six CTD sections at longitudes spanning the Pacific and for which the geostrophic relative velocities were referenced using shipboard ADCPs. The uncertainties in the *Donohue et al.* [2001] estimates were quite large in some cases however, exceeding 25% of the absolute transport for one of the sections. *Whitworth* [1983] found that averaged over about a year the barotropic contribution to the absolute ACC transport through Drake Passage was roughly 25%, although that study defined the baroclinic transport relative to the fairly shallow level of 2500 dbar. It should be reiterated that while the SAFDE stream coordinates mean section had a fairly small barotropic component, at times the deep flows were much larger and resulted in barotropic transports of 30–40 Sv [*Meinen et al.*, 2002; *Meinen and Luther*, 2003].

4.12. Diffluent Transport

[39] The transport discussion up to this point has focused on the along-stream flow. However, one of the most unexpected results from this study is the presence of a strong cross-stream diffluence over the full water column with a significant baroclinic component (Figure 5). This diffluence, if maintained over a significant along-stream distance, would result in either a significant widening of the current or a substantial decrease in the flow along the SAF due to conservation of mass. Combining the diffluent transport to the north and south across +80 km and −80 km on the cross-stream distance axis, it is found that the core SAF within these distances is losing 0.23 Sv per kilometer or roughly 16 Sv per degree of longitude at 51°S. As this represents a significant fraction of the absolute along-stream transport, it seems extremely unlikely that this cross-stream diffluence is maintained over a long distance along the front. For comparison purposes, Gulf Stream transport

appears to decrease by 6 Sv per degree of longitude between 55°W and 50°W [*Meinen*, 2001].

[40] *Rintoul et al.* [2001] have proposed a recirculation gyre north of the SAF but they do not envision any recirculation to the south. The northern component of the cross-stream diffluence based on Figure 5a is about 70% larger than the southern component at equal distances from the core. Nevertheless, the latter comprises just under 40% of the total cross-stream diffluence, which therefore suggests that there must be a significant recirculation or broadening to the south of the SAF as well. The second front to the south of the SAF (see Figure 1) may contribute to the observed southward transport; however, as noted earlier, if the time periods when the second front is clearly present in the OI mapping region are excluded from the stream coordinates averaging, the mean southward flow decreases but does not disappear (the southward transport change is less than 20%). Therefore the southward diffluence appears robust. A southern recirculation is unlikely given that neither the PR02 stream coordinates section nor the SAFDE section indicates a reversal of flow to westward on the south side of the SAF. Additionally, the Eulerian mean velocities from several HEFRs that extended farther south than the SAFDE main array (see Figure 1) showed no indication of westward flow. Whether the southward diffluent flow reconnects with the southeastward trending SAF core farther downstream, or connects with the flow along the PF and is somehow compensated upstream by fluid leaving the PF to join the flow along the SAF, or whether there is a tight recirculation gyre south of the SAF at this location which is obscured in the Eulerian averaging of the HEFR measurements, are questions which will require further study.

5. Summary and Concluding Remarks

[41] Using 2 years of temperature, salinity, and absolute velocity profiles obtained from the combination of hydrography, IESs, and HEFRs, a stream coordinates representation of the temperature, salinity, and absolute velocity of the SAF has been developed. These sections represent the most complete description to date of the SAF and its flow. The flow along the SAF has been shown to have a single peak with a maximum mean speed of about 50 cm s^{-1} and a near-bottom mean speed of up to 2 cm s^{-1}. Over the maximum horizontal span (220 km) of our observations the mean absolute transport along the SAF during the two year (March 1995 to April 1997) period of the experiment was about 75 Sv based on the stream coordinates mean section. The cross-stream flow was baroclinically diffluent (relative to the bottom), while the barotropic (bottom velocity) component of the cross-stream flow was essentially all weakly northward across the front with a diffluent tendency. The total cross-stream diffluence is significant based on the estimated measurement and statistical error bars, and the peak speeds of the cross-stream diffluent flows are roughly equal on both sides of the SAF.

[42] The barotropic component of the along-stream transport is found to be fairly small in the stream coordinates mean, contrary to prior investigations of the SAF at other longitudes. SAFDE current time series indicate that at times there were very significant bottom velocities (e.g., Figure 2), which may explain the difference between the weak SAFDE mean barotropic flow and the stronger barotropic flows observed by others using a few snapshot sections [e.g., *Donohue et al.*, 2001]. The SAFDE results also indicate a narrower current along the SAF than was estimated by the only other stream coordinates study of the SAF (PR02).

[43] The SAFDE study has demonstrated that an array of IESs, when combined with additional measurements such as the HEFRs for absolute referencing the geostrophic relative velocities, provides a powerful and relatively inexpensive method for determining the structure and transport along a Southern Ocean front. It is quite reasonable, given this technology, to monitor the structure and transport of the entire ACC flow through the Drake Passage, for instance, with a coherent Antarctica-to-South America array of IESs and HEFRs. At other locations around the Southern Ocean, where the ACC is not as constrained as it is in the Drake Passage "chokepoint," lines of IESs could still be deployed to span the entire ACC by using closer meridional instrument spacing in the regions where fronts are expected and wider spacing at other latitudes. The geostrophic transports derived by the IESs would naturally integrate across the distances between instruments. As such, the IES represents a powerful instrument for future studies of the ACC.

Appendix A: Error Analysis

[44] *Meinen et al.* [2002] quantify the accuracy for each daily estimate of the absolute velocities derived from the IES and HEFR measurements to be 8, 6, 4, and 3 cm s^{-1} for pressures of 300, 600, 1000, and 2000 dbar, respectively. In order to determine the accuracy of the stream coordinates mean values shown in Figure 4, an estimate of the degrees of freedom must be made. *Johns et al.* [1995] showed that the number of degrees of freedom in a stream coordinates reference frame was essentially the same as for an Eulerian reference frame. This makes sense, because although moving to a stream coordinates reference frame eliminates the horizontal motion of the meanders, it does not eliminate the changes in thermocline slope which are associated with the changes in curvature due to the meanders [e.g., *Watts et al.*, 1995, their Figure 10]. The number of degrees of freedom across the section was determined as follows. First, the integral timescale of vertically averaged horizontal velocity was determined at each of the HEFR sites [*Emery and Thomson*, 1997], yielding an average integral timescale of about 11 days. Next, because the "time series" of points available in each stream coordinates averaging bin was irregular (ranging from three to four points in a single bin on a given day, if the SAF was running parallel to the HEFR line that day, to no observations in a particular bin for weeks), it was necessary to break up the time series for each cross-stream bin into sections one integral timescale in length and then determine how many of the sections contained observations. The resulting number of degrees of freedom ranged from 6 to 20, with the fewest number on the warm side of the SAF and the larger number on the cold side of the SAF (Figure 4d). Near the SAF core, there were about 14 degrees of freedom, which indicates that the measurement errors contribute at most 1–2 cm s^{-1} to the error in the stream coordinates mean. Near the SAF core the statistical standard

error of the mean, defined here as the standard deviation divided by the square root of the number of degrees of freedom, ranges from 2 cm s^{-1} at 2000 dbar to 7 cm s^{-1} near the surface for the along-stream velocities and 1 cm s^{-1} at 2000 dbar to 2 cm s^{-1} near the surface for the cross-stream velocities. Therefore, combining the measurement and statistical error bars, the mean velocities shown in Figures 4 and 5 are accurate to within 7 cm s^{-1} near the surface. Below 2000 dbar the accuracy improves to better than 2 cm s^{-1}.

[45] Below the upper 100–200 dbar, where seasonal variability is large, the daily estimates of temperatures and salinities are accurate to within 0.05–0.4°C and 0.005–0.05 psu, respectively, with the errors due primarily to the scatter about the GEM temperature and salinity fields. Including the standard error of the mean, and assuming the same number of degrees of freedom as for the velocity observations, the time mean temperature (salinity) section is accurate to within 0.1°C (0.02 psu) within the main thermocline (halocline) and to within 0.015°C (0.001 psu) below 2000 dbar.

[46] **Acknowledgments.** The authors would like to thank Steve Rintoul for providing some of the hydrography used in this study and Sarah Gille for providing her SAF and PF frontal positions. Helen Phillips kindly provided her estimates of the stream coordinates mean along-stream velocity. Helen Phillips, Steve Rintoul, Bill Johns, Mindy Hall, and Molly Baringer provided numerous helpful comments during discussions regarding the nature of stream coordinates. David Webb and Nathan Bindoff made many helpful suggestions for improving this manuscript. The Sub-Antarctic Flux and Dynamics Experiment (SAFDE) was designed by Alan Chave, Jean Filloux, Doug Luther, Jim Richman, and Randy Watts, in collaboration with John Church and Steve Rintoul, after discussions with Eric J. Lindstrom in 1990. SAFDE was funded in the U.S. under NSF grants OCE92-04063, OCE92-04113, OCE92-04041, OCE99-12110, OCE99-12320, and OCE99-11974.

References

Best, S. E., V. O. Ivchenko, K. J. Richards, R. D. Smith, and R. C. Malone, Eddies in numerical models of the Antarctic Circumpolar Current and their influence on the mean flow, *J. Phys. Oceanogr.*, *29*, 328–350, 1999.

Bower, A. S., and N. G. Hogg, Structure of the Gulf Stream and its recirculations at 55°W, *J. Phys. Oceanogr.*, *26*, 1002–1022, 1996.

Bretherton, F. P., R. E. Davis, and C. B. Fandry, A technique for objective analysis and design of oceanographic experiments applied to MODE-73, *Deep Sea Res., Part I*, *23*, 559–582, 1976.

Bryden, H. L., Poleward heat flux and conversion of available potential energy in Drake Passage, *J. Mar. Res.*, *37*, 1–22, 1979.

Bryden, H. L., and R. A. Heath, Energetic eddies at the northern edge of the Antarctic Circumpolar Current in the southwest Pacific, *Prog. Oceanogr.*, *14*, 65–87, 1985.

Chaplin, G. F., and D. R. Watts, Inverted echo sounder development, in *IEEE Oceans '84 Conference Record*, vol. 1, pp. 249–253, Inst. of Elect. and Elect. Eng., New York, 1984.

Chave, A. D., and D. S. Luther, Low-frequency, motionally induced electromagnetic fields in the ocean: 1. Theory, *J. Geophys. Res.*, *95*, 7185–7200, 1990.

Chelton, D., M. G. Schlax, D. L. Witter, and J. G. Richman, Geosat altimeter observations of the surface circulation of the Southern Ocean, *J. Geophys. Res.*, *95*, 17,877–17,903, 1990.

Cushman-Roisin, B., *Introduction to Geophysical Fluid Dynamics*, Prentice-Hall, Old Tappan, N. J., 1994.

Donohue, K. A., E. Firing, and S. Chen, Absolute geostrophic velocity within the Subantarctic Front in the Pacific Ocean, *J. Geophys. Res.*, *106*, 19,869–19,882, 2001.

Emery, W. J., and R. E. Thomson, *Data Analysis Methods in Physical Oceanography*, Pergamon, New York, 1997.

Fofonoff, N. P., Dynamics of ocean currents, in *The Sea: Ideas and Observations on Progress in the Study of the Seas*, vol. 1, *Physical Oceanography*, edited by M. N. Hill, pp. 323–395, Wiley-Intersci., New York, 1962.

Fofonoff, N. P., and M. M. Hall, Estimates of mass, momentum and kinetic energy fluxes of the Gulf Stream, *J. Phys. Oceanogr.*, *13*, 1868–1877, 1983.

Gille, S. T., Mean sea surface height of the Antarctic Circumpolar Current from Geosat data: Method and application, *J. Geophys. Res.*, *99*, 18,255–18,273, 1994.

Grose, T. J., J. A. Johnson, and G. R. Bigg, A comparison between the FRAM (Fine Resolution Antarctic Model) results and observations in the Drake Passage, *Deep Sea Res., Part I*, *42*, 365–388, 1995.

Halkin, D., and H. T. Rossby, The structure and transport of the Gulf Stream at 73°W, *J. Phys. Oceanogr.*, *15*, 1439–1452, 1985.

Hall, M. M., Horizontal and vertical structure of the Gulf Stream velocity field at 68°W, *J. Phys. Oceanogr.*, *16*, 1814–1828, 1986.

Hall, M. M., Velocity and transport structure of the Kuroshio Extension at 35°N, 152°E, *J. Geophys. Res.*, *94*, 14,445–14,459, 1989.

Hall, M. M., and H. L. Bryden, Profiling the Gulf Stream with a current meter mooring, *Geophys. Res. Lett.*, *12*, 203–206, 1985.

Hanawa, K., L. D. Talley, Mode waters, in *Ocean Circulation and Climate*, chap. 5.4, pp. 373–386, Academic Press, San Diego, Calif., 2001.

Hofmann, E. E., The large-scale horizontal structure of the Antarctic Circumpolar Current from FGGE drifters, *J. Geophys. Res.*, *90*, 7087–7097, 1985.

Hogg, N. G., On the transport of the Gulf Stream between Cape Hatteras and the Grand Banks, *Deep Sea Res., Part I*, *39*, 1231–1246, 1992.

Inoue, M., Modal decomposition of the low-frequency currents and baroclinic instability at Drake Passage, *J. Phys. Oceanogr.*, *15*, 1157–1181, 1985.

Johns, W. E., T. J. Shay, J. M. Bane, and D. R. Watts, Gulf Stream structure, transport, and recirculation near 68°W, *J. Geophys. Res.*, *100*, 817–838, 1995.

Kontoyiannis, H., Quasi-geostrophic modeling of mixed instabilities in the Gulf Stream near 73°W, *Dyn. Atmos. Oceans*, *26*, 133–158, 1997.

Luther, D. S., J. H. Filloux, and A. D. Chave, Low-frequency, motionally induced electromagnetic fields in the ocean: 2. Electric field and eulerian current comparison, *J. Geophys. Res.*, *96*, 12,797–12,814, 1991.

Luther, D. S., A. D. Chave, J. A. Church, J. H. Filloux, J. G. Richman, S. R. Rintoul, and D. R. Watts, The sub-antarctic flux and dynamics experiment (SAFDE), *WOCE Notes*, *9*, 8–12, 1997.

Meinen, C. S., Structure of the North Atlantic Current in stream-coordinates and the circulation in the Newfoundland Basin, *Deep Sea Res., Part I*, *48*, 1553–1580, 2001.

Meinen, C. S., and D. S. Luther, Comparison of methods of estimating mean synoptic current structure in "stream coordinates" reference frames with an example from the Antarctic Circumpolar Current, *Deep Sea Res., Part I*, *50*, 201–220, 2003.

Meinen, C. S., and D. R. Watts, Vertical structure and transport on a transect across the North Atlantic Current near 42°N: Time series and mean, *J. Geophys. Res.*, *105*, 21,869–21,891, 2000.

Meinen, C. S., D. S. Luther, D. R. Watts, K. L. Tracey, A. D. Chave, and J. Richman, Combining Inverted Echo Sounder and Horizontal Electric Field Recorder measurements to obtain absolute velocity profiles, *J. Atmos. Oceanic Technol.*, *19*, 1653–1664, 2002.

Mestas-Nunez, A., D. B. Chelton, and R. A. DeSzoeke, Evidence of time-dependent Sverdrup circulation in the South Pacific from the Seasat scatterometer and altimeter, *J. Phys. Oceanogr.*, *22*, 934–943, 1992.

Moore, J. K., M. R. Abbott, and J. G. Richman, Variability in the location of the Antarctic Polar Front (90°–20°W) from satellite sea surface temperature data, *J. Geophys. Res.*, *102*, 27,825–27,833, 1997.

Moore, J. K., M. R. Abbott, and J. G. Richman, Location and dynamics of the Antarctic Polar Front from satellite sea surface temperature data, *J. Geophys. Res.*, *104*, 3059–3073, 1999.

Morrow, R., R. Coleman, J. Church, and D. Chelton, Surface eddy momentum flux and velocity variances in the Southern Ocean from Geosat altimetry, *J. Phys. Oceanogr.*, *24*, 2050–2071, 1994.

Nowlin, W. D., Jr., and M. Clifford, The kinematic and thermohaline zonation of the Antarctic Circumpolar Current at Drake Passage, *J. Mar. Res.*, *40*, 481–507, 1982.

Nowlin, W. D., Jr., and J. M. Klinck, The physics of the Antarctic Circumpolar Current, *Rev. Geophys.*, *24*, 469–491, 1986.

Orsi, A. H., T. Whitworth III, and W. D. Nowlin Jr., On the meridional extent and fronts of the Antarctic Circumpolar Current, *Deep Sea Res., Part I*, *42*, 641–673, 1995.

Park, Y.-H., and L. Gamberoni, Large-scale circulation and its variability in the south Indian Ocean from TOPEX/POSEIDON altimetry, *J. Geophys. Res.*, *100*, 24,911–24,929, 1995.

Philander, S. G. H., Forced oceanic waves, *Rev. Geophys.*, *16*, 15–46, 1978.

Phillips, H. E., and S. R. Rintoul, Eddy variability and energetics from direct current measurements in the Antarctic Circumpolar Current south of Australia, *J. Phys. Oceanogr.*, *30*, 3050–3076, 2000.

Phillips, H. E., and S. R. Rintoul, A mean synoptic view of the Subantarctic Front south of Australia, *J. Phys. Oceanogr.*, *32*, 1536–1553, 2002.

Read, J. F., R. T. Pollard, A. I. Morrison, and C. Symon, On the southerly extent of the Antarctic Circumpolar Current in the southeast Pacific, *Deep Sea Res., Part II*, *42*, 933–954, 1995.

Rintoul, S. R., and S. Sokolov, Baroclinic transport variability of the Antarctic Circumpolar Current south of Australia (WOCE repeat section SR3), *J. Geophys. Res.*, *106*, 2815–2832, 2001.

Rintoul, S. R., C. Hughes, and D. Olbers,The Antarctic Circumpolar Current system, in *Ocean Circulation and Climate*, chap. 4.6, pp. 271–302, Academic Press, San Diego, Calif., 2001.

Rossby, T., On the energetics of the Gulf Stream at 73W, *J. Mar. Res.*, *45*, 59–82, 1987.

Rossby, T., and H.-M. Zhang, The near-surface velocity and potential vorticity structure of the Gulf Stream, *J. Mar. Res.*, *59*, 949–975, 2001.

Sanford, T. B., Motionally-induced electric and magnetic fields in the sea, *J. Geophys. Res.*, *76*, 3476–3492, 1971.

Sinha, B., and K. J. Richards, Jet structure and scaling in Southern Ocean models, *J. Phys. Oceanogr.*, *29*, 1143–1155, 1999.

Smith, R. D., M. E. Maltrud, F. O. Bryan, and M.W. Hecht, Numerical simulation of the North Atlantic Ocean at 1/10°, *J. Phys. Oceanogr.*, *30*, 1532–1561, 2000.

Smith, W. H. F., and D. T. Sandwell, Global sea floor topography from satellite altimetry and ship depth soundings, *Science*, *277*, 1956–1962, 1997.

Sokolov, S., and S. R. Rintoul, Structure of southern ocean fronts at 140°E, *J. Mar. Syst.*, *37*, 151–184, 2002.

Stammer, D., Global characteristics of ocean variability estimated from regional TOPEX/POSEIDON altimeter measurements, *J. Phys. Oceanogr.*, *27*, 1743–1768, 1997.

Sun, C., and D. R. Watts, A circumpolar gravest empirical mode for the Southern Ocean hydrography, *J. Geophys. Res.*, *106*, 2833–2856, 2001.

Tomczak, M., and J. S. Godfrey, *Regional Oceanography: An Introduction*, Pergamon, New York, 1994.

Treguier, A. M., and R. L. Panetta, Multiple zonal jets in a quasigeostrophic model of the Antarctic Circumpolar Current, *J. Phys. Oceanogr.*, *24*, 2263–2277, 1994.

Watts, D. R., and H. T. Rossby, Measuring dynamic heights with inverted echo sounders: Results from MODE, *J. Phys. Oceanogr.*, *7*, 345–358, 1977.

Watts, D. R., K. L. Tracey, J. M. Bane, and T. J. Shay, Gulf Stream path and thermocline structure near 74°W and 68°W, *J. Geophys. Res.*, *100*, 18,291–18,312, 1995.

Watts, D. R., C. Sun, and S. Rintoul, A two-dimensional gravest Empirical Mode determined from hydrographic observations in the Subantarctic Front, *J. Phys. Oceanogr.*, *31*, 2186–2209, 2001.

Whitworth, T., III, Monitoring the transport of the Antarctic Circumpolar Current at Drake Passage, *J. Phys. Oceanogr.*, *13*, 2045–2057, 1983.

Whitworth, T., III, and W. D. Nowlin Jr., Water masses and currents of the Southern Ocean at the Greenwich Meridian, *J. Geophys. Res.*, *92*, 6462–6476, 1987.

Whitworth, T., III, W. D. Nowlin Jr., and S. J. Worley, The net transport of the Antarctic Circumpolar Current through Drake Passage, *J. Phys. Oceanogr.*, *12*, 960–971, 1982.

Yaremchuk, M., N. L. Bindoff, J. Schröter, D. Nechaev, and S. R. Rintoul, On the zonal and meridional circulation and ocean transports between Tasmania and Antarctica, *J. Geophys. Res.*, *106*, 2795–2814, 2001.

A. D. Chave, Deep Submergence Laboratory, Applied Ocean Physics and Engineering, Woods Hole Oceanographic Institution, Woods Hole, MA 02543, USA. (achave@whoi.edu)

D. S. Luther, Department of Oceanography, University of Hawaii at Manoa, 1000 Pope Road, MSB 205, Honolulu, HI 96822, USA. (dluther@soest.hawaii.edu)

C. S. Meinen, NOAA/AOML/PHOD, 4301 Rickenbacker Causeway, Miami, FL 33149, USA. (Christopher.Meinen@noaa.gov)

K. L. Tracey and D. R. Watts, Graduate School of Oceanography, University of Rhode Island, 215 South Ferry Road, Narragansett, RI 02882, USA. (ktracey@gso.uri.edu; rwatts@gso.uri.edu)